

Analysis of low-frequency wave scattering by turbulent premixed flame

JU HYEONG CHO†

School of Aerospace Engineering, Georgia Institute of Technology, Atlanta, GA 30332-0150, USA

(Received 25 April 2007 and in revised form 17 March 2009)

Theoretical investigation of acoustic wave interactions with turbulent premixed flames was conducted to evaluate the acoustic energy amplification and/or damping due to the interaction of low-frequency acoustic waves with turbulent flames in three-dimensional space. Such amplified or damped acoustic energy is either coherent or incoherent as wrinkled flames cause coherent energy of a monochromatic acoustic wave to be damped into incoherent energy of spatially diffused and spectrally broadened acoustic waves. Small perturbation method (SPM) up to the second order was utilized to analyse net coherent and incoherent acoustic energies of the reflected and transmitted waves scattered from a weakly wrinkled turbulent flame surface in random motion. General formulations for net coherent and incoherent energy budget of the scattered fields were derived that can be applied to any type of flame height statistics. Production and/or damping of acoustic energy scattered from a turbulent flame is attributed to two effects: one is the acoustic velocity jump due to flame's unsteady heat release and the other is the flame's wrinkling due to its unsteady motion. Dimensionless parameters that govern net acoustic energy budget were derived in case of Gaussian statistics of flame surface behaviour: the r.m.s. and correlation length of flame height, the frequency ratio of the incidence frequency to the flame's correlation frequency, the time ratio of the flame's diffusion to correlation time and the incidence angle. The results of the scattered acoustic energy budget showed that noticeable amplification of acoustic energy was obtained either for a small frequency ratio ($\ll 1$) at the critical incidence angle or for a large frequency ratio and time ratio ($\gg 1$), while damping was obtained for a small frequency ratio at off-critical incidence angles. The relative importance of unsteady heat release (the jump effect) and unsteady motion (the wrinkling effect) to net acoustic energy is controlled mainly by the frequency ratio: The unsteady heat release effect dominates the wrinkling effect at a large frequency ratio, and vice versa at a small frequency ratio. The energy transfer from coherent to incoherent energy is due to flame surface wrinkling and is enhanced with the square of the flame's r.m.s. height.

1. Introduction

This paper deals with the analysis of acoustic wave interactions with turbulent premixed flames. Such interactions play an important role in many fundamental and practical problems in various combustion and propulsion systems. For instance, those interactions affect the characteristic unsteadiness of combustion processes and play

† Present address: Korea Institute of Machinery and Materials, Daejeon, Republic of Korea.
Email address for correspondence: antocho@hanmail.net

a crucial role in the problem of combustion instabilities, which have been known to arise from the interactions between acoustic waves and combustion processes which occur in a self-exciting manner at lean premixed conditions (Putnam 1971; Lieuwen & Yang 2005). Acoustic wave–flame interactions have been considered in a large number of theoretical and experimental studies so far. Theoretical treatment of the acoustic wave–flame interaction phenomena was initiated by Chu (1952), who regarded the flame front as a temperature discontinuity that separates the unburned reactants from the burned products. Markstein (1964) also analysed the effects of unsteady small perturbations upon a steady-state planar flame by treating the flame front as a surface of discontinuity and applying the first-order perturbation methods to linearize the conservation equations of mass, momentum and energy and flame kinematic equations. These works have been extended in several analyses, such as those of McIntosh (1987, 1991, 1999) and McIntosh & Wilce (1991), Peters & Ludford (1983) and Ledder & Kapila (1991), which assessed the effects of pressure perturbations on the unsteady inner flame structure. Other analyses incorporating the coupling effects between the acoustic wave and the burning-rate fluctuations have also been reported by Clavin, Pelce & He (1990), Poinsoot & Candel (1988), Lieuwen (2001*a*) and others. Another important process in these interactions, i.e. the periodic acceleration and/or convection of the flame front by the oscillatory flow field, has been discussed by Markstein (1964), Searby & Rochwerger (1991) and Fleifil *et al.* (1996).

There are three canonical modes of disturbances, i.e. acoustic, entropy and vorticity modes which become strongly coupled at the flame front (Chu & Kovaszny 1958). The acoustic wave–flame interactions are manifested by amplification or damping of acoustic waves via energy transfer among these three disturbance modes. Theoretical investigations were reported by McIntosh (1987), Poinsoot & Candel (1988), Lieuwen (2001*a*) and others. McIntosh (1987) reported that the low-frequency acoustic wave amplification is sensitive to the impedance at the burner surface. More recently, Lieuwen (2001*a*) reported two-dimensional analysis by considering acoustic waves that are obliquely incident upon the planar flame front. He demonstrated that net acoustic energy out of the flame is controlled by competition between acoustic energy production and dissipation processes. Energy addition is due to unsteady heat release through fluctuations in flame speed or density while energy damping is due to baroclinic production of vorticity. He reported that such amplification/damping of acoustic energy is more complicated process which results from the combined effects of refraction, temperature jump across the flame, vorticity production and flame speed modulation, and so on. Other researchers, for instance, Poinsoot *et al.* (1987), Bloxside *et al.* (1988) and McManus, Poinsoot & Candel (1993), reported estimations of amplification or damping of acoustic waves by utilizing Rayleigh's criterion to evaluate local or global instability associated with combustion–acoustic wave interactions. (Rayleigh's criterion states that acoustic waves will be locally amplified (damped) if acoustic pressure is in phase (out of phase) with flame's heat release oscillations.)

The primary emphasis of the theoretical work mentioned above is to model the laminar flame–acoustic wave interaction problems. Searby & Clavin (1986) performed theoretical analysis to examine the dynamic behaviour of a wrinkled flame front propagating downwards in a weakly turbulent flow. Coupled linearized forms of continuity, momentum and flame's kinematic equations are solved to evaluate the mutual interactions between wrinkled flame and turbulent flow field in terms of Froude number (gravity effect) and Markstein number (flame's curvature effect). They applied jump conditions of pressure and velocity across the mean flame surface

to calculate amplification/damping of flow velocity and flame position. However, fluctuation quantities of flame front position, pressure and velocity are assumed to follow harmonic oscillation and, therefore, stochastic analysis associated with the random effect of turbulent flames is not actually incorporated. Furthermore, the boundary conditions are applied to the mean flame surface, not to its instantaneous position. Several more recent studies (Lieuwen 2001*b*, 2002; Lieuwen & Cho 2005) have extended the developed analysis based on the laminar flame to the problems of acoustic wave interaction with turbulent flames by applying stochastic analysis to account for randomly wrinkling turbulent flames. They analysed the high-frequency acoustic wave scattering from single-connected wrinkled flame fronts by modelling the flame as a dynamically evolving wrinkled temperature discontinuity. Their results suggest that several qualitative differences exist between the characteristics of scattering waves from laminar and turbulent flames. Most significance of these results is the fact that a coherent harmonically oscillating acoustic wave incident upon a turbulent flame generates both coherent and incoherent scattered waves. This is due to the characteristics of the wrinkled turbulent flame that transmits coherent acoustic energy into diffuse incoherent energy. Moreover, with increasing the roughness σ/λ (σ : the standard deviation of roughness, λ : acoustic wavelength), the power of the coherent field decreases and, subsequently, the power of the incoherent field increases, at least for small σ/λ . The above-mentioned studies about acoustic–turbulent flame interaction are based on the assumption of high-frequency acoustic waves, which utilized the Kirchoff approximation, or the tangent plane approximation, where the flame front locally looks planar to the short-wavelength acoustic wave. However, combustion instabilities have also been reported to be often observed in a low-frequency regime. For example, both aeroderivatives (liquid rockets) and land-based gas turbines were reported to suffer from combustion instabilities within 500 Hz frequency range (Lieuwen & Yang 2005, chapters 1 and 7). Hence the flame interactions with low-frequency acoustic waves are also regarded as being consequential in the context of combustion instabilities. The aim of the present study is to reveal the characteristics of low-frequency acoustic waves–turbulent flame interactions by utilizing small perturbation method (SPM) to examine how much coherent and incoherent acoustic energy is amplified and/or damped by the interaction of a low-frequency wave with a turbulent flame and identify the key parameters controlling the acoustic energy amplification and/or damping. The scope of the present study is as follows: Section 2 introduces the scattering amplitudes and evaluates them using SPM with the second-order accuracy and derives formulations of the scattered acoustic energy budget. Section 3 demonstrates analytical and numerical results to quantitatively examine the characteristics of net acoustic energy budget. Concluding remarks are in §4.

2. Analysis

2.1. Problem statement and basic assumptions

Figure 1 illustrates the schematics where plane incident waves impinge upon a randomly moving wrinkled flame surface and, subsequently, scattered waves are reflected and transmitted by the flame. The problems of interest are associated with

- (i) how the scattered, i.e. reflected and transmitted, acoustic fields are characterized in terms of the incident wave field and the flame's kinematics quantities,
- (ii) how the acoustic energy is amplified and/or damped after scattering, and how net acoustic energy of the scattered fields can be obtained quantitatively and

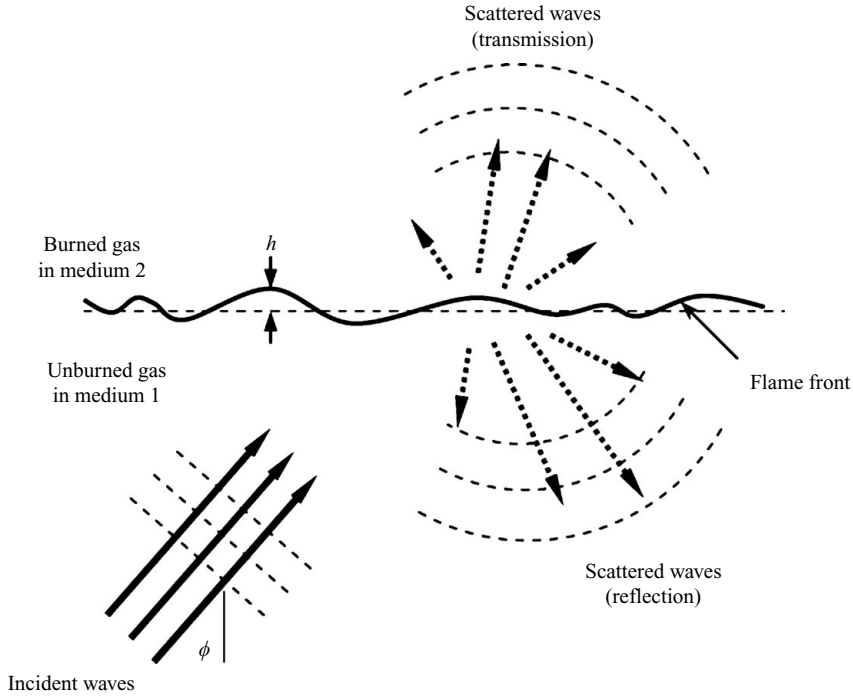


FIGURE 1. Schematic illustration of a flame surface in acoustic fields.

(iii) what key factors influence the net coherent and incoherent energies of scattered wave fields.

Several assumptions are made to render the theoretical approach tractable.

(i) The height and slope of a wrinkled flame surface are small (see (2.20)).

(ii) The flame extends without boundary. This assumption is equivalent to neglecting edge effects, such as diffraction from the flame edges.

(iii) Multiple scattering is not considered, i.e. all scattering is assumed to be single scattering. This assumption, called Rayleigh's hypothesis, is known to yield the same result as the exact solution as long as the slope of the rough surface is sufficiently small; e.g. if the maximum slope of surface is not greater than 0.448 for the Dirichlet problem (Voronovich 1999). The assumption of single scattering implies that the present analysis applies to wrinkled flamelets, not to corrugated flamelets where multiple scattering will be present.

(iv) The flame front is temperature discontinuity that separates the unburned reactants and burned products.

(v) Vorticity and entropy modes are neglected in the present analysis. In fact, neglecting the vorticity mode can lead to a significant overestimation of the acoustic energy production by flames in some cases. For example, the vorticity produced by the interaction between a laminar flame and acoustic waves can damp as much as 14% of the incident acoustic energy when an incident wave is impinging on a flame at the critical (cut-off) angle, as is demonstrated by Lieuwen (2001). This is typical of hydrogen-rich flames where the flame speed Mach number is usually above 0.005. For typical hydrocarbon flames, flame speed is much lower; e.g. the flame speed Mach number for a stoichiometric methane/air flame is about 0.001. In this case, acoustic

damping due to vorticity production is less than 3% of the incident acoustic energy for all angles of incidence.

In realistic situations the overall net acoustic energy provided by the turbulent flame–acoustic wave interaction is likely to be determined by the complex nature of the combined effects among acoustic processes, unsteady heat release, turbulent flame wrinkling, vorticity production and so on. Therefore, full consideration of all of these effects still poses a quite challenging task. As such, this paper makes no attempt to address all of these effects. Rather, the present analysis focuses on acoustic processes with consideration of unsteady heat release and wrinkling by turbulent flame, but without consideration of vorticity mode, as the specific objective of the present study is to provide general formulations for net coherent and incoherent acoustic energy budget of the scattered fields by the turbulent flame–acoustic wave interaction.

2.2. Scattered acoustic fields and boundary conditions

The linearized wave equation in terms of the velocity potential ψ and sound sources Q is of the form

$$\left(\nabla^2 - \frac{1}{c^2} \frac{\partial^2}{\partial t^2} \right) \psi(\mathbf{R}, t) = Q(\mathbf{R}, t), \quad (2.1)$$

where c is the speed of sound, t is time, $\nabla^2 = \partial_{xx} + \partial_{yy} + \partial_{zz}$, $\mathbf{R} = (x, y, z)$. ψ , velocity potential, is related to the acoustic velocity \mathbf{v} and acoustic pressure p as

$$\mathbf{v} = \nabla \psi(\mathbf{R}, t), \quad p = -\rho_0 \frac{\partial \psi(\mathbf{R}, t)}{\partial t}, \quad (2.2)$$

where ∇ is three-dimensional gradient ($= (\partial_x, \partial_y, \partial_z)$), the acoustic pressure was obtained from the linearized Euler's equation, $\rho_0 \partial \mathbf{v} / \partial t = -\nabla p$. The solution of a linearized wave equation can be expressed in terms of superposition of elementary plane waves as utilized by Voronovich (1999). The present analysis utilizes his approach but incorporates frequency domain analysis to account for the frequency shift due to the flame's unsteady effect, which is not considered by Voronovich. Consider media 1 and 2 that are separated by a (flame front) boundary as shown in figure 1. Let the incident wave be a plane wave that is propagating in medium 1 with a horizontal component of wavenumber vector \mathbf{k}_0 and angular frequency ω_0 and impinging upward upon the (flame front) boundary. Then the total acoustic fields in each medium can be described by the following forms:

$$\text{In medium } (m), \quad \psi^{(m)}(\mathbf{R}, t) = \text{Re}[\psi_c^{(m)}] \quad (m = \{1, 2\}) \quad (2.3)$$

$$\begin{aligned} \frac{\psi_c^{(1)}}{A} &= (\rho_1 q_0^{(1)})^{-1/2} e^{i(\mathbf{k}_0 \cdot \mathbf{r} + q_0^{(1)} z - \omega_0 t)} + \int_{\omega} \int_{\mathbf{k}} S^{11}(\mathbf{k}, \mathbf{k}_0, \omega, \omega_0) \\ &\quad \times (\rho_1 q_k^{(1)})^{-1/2} e^{i(\mathbf{k} \cdot \mathbf{r} - q_k^{(1)} z - \omega t)} d\mathbf{k} d\omega, \end{aligned} \quad (2.4)$$

$$\frac{\psi_c^{(2)}}{A} = \int_{\omega} \int_{\mathbf{k}} S^{21}(\mathbf{k}, \mathbf{k}_0, \omega, \omega_0) (\rho_2 q_k^{(2)})^{-1/2} e^{i(\mathbf{k} \cdot \mathbf{r} + q_k^{(2)} z - \omega t)} d\mathbf{k} d\omega \quad (2.5)$$

$$A = \frac{|P_I|}{i\omega_0} \left(\frac{q_0^{(1)}}{\rho_1} \right)^{1/2}, \quad q_0^{(1)} = [(\omega_0/c_1)^2 - k_0^2]^{1/2}, \quad q_k^{(m)} = [(\omega/c_m)^2 - k^2]^{1/2} \quad (m = \{1, 2\}),$$

$$k = |\mathbf{k}|, \quad \mathbf{r} = (x, y),$$

where ρ_1, c_1 and ρ_2, c_2 are density and sound speed in media 1 and 2, respectively, P_I is a complex amplitude of an incident wave pressure, and $q_0^{(1)}, q_k^{(1)}$ and $q_k^{(2)}$ are the vertical wavenumber components of the incident and scattered waves in each medium. $(\rho_1 q_k^{(1)})^{-1/2}$ in (2.4) and $(\rho_2 q_k^{(2)})^{-1/2}$ in (2.5) result from rendering the energy

flux along the z -axis to be constant and \mathbf{k} independent (Voronovich 1999). These can be complex when $\omega/c < k$, representing exponentially decaying waves. S^{11} and S^{21} will be evaluated from the boundary conditions on the flame front where $S^{N_1 N_2}$ denotes the scattering amplitude of waves that are scattered into medium N_1 by incident waves from medium N_2 . Therefore, $S^{11}(S^{21})$ is related to the reflected (transmitted) waves.

Boundary conditions at the flame front are characterized by jump conditions in acoustic pressure and velocity due to unsteady gas expansion from a flame front. These jump conditions have been derived by many researchers using conservation relations and reported to be expressed as mean flame speed Mach number for unburned gas, $M_S (= \bar{S}_L^{(1)}/c_1)$, and perturbations in mass burning rate and pressure (Chu 1952; McIntosh 1991; Lieuwen 2001a). The jump condition in a linearized acoustic pressure p_1 across a flame front is of the order of $O(M_S^2)$, i.e. $p_1^{(1)} = p_1^{(2)} + O(M_S^2)$ (Lieuwen 2001a) and, therefore, is reduced to the continuity condition, $p_1^{(1)} = p_1^{(2)}$, of the order of $O(M_S)$, which is also expressed in terms of velocity potential using (2.2).

$$\rho_1 \left. \frac{\partial \psi_c^{(1)}(\mathbf{R}, t)}{\partial t} \right|_{z=h(r,t)} = \rho_2 \left. \frac{\partial \psi_c^{(2)}(\mathbf{R}, t)}{\partial t} \right|_{z=h(r,t)}, \quad (2.6)$$

where h is a perturbation in flame height. The velocity jump condition at the flame front can be obtained from the linearized energy equation. For instance, the energy equation was linearized by Lieuwen (2001a).

$$\frac{v_{1,n}^{(2)}}{c_1} - \frac{v_{1,n}^{(1)}}{c_1} = M_S \left(\frac{(\gamma + \Lambda - 1) p_1^{(1)}}{\gamma p_0} - \Lambda \frac{p_1^{(2)}}{p_0} + (\Lambda - 1) \frac{S_{L,1}^{(1)}}{S_{L,0}^{(1)}} \right) + O(M_S^2), \quad (2.7)$$

where $v_{1,n}$ denotes a linearized acoustic velocity that is normal to a wrinkled flame surface, $S_{L,0}^{(1)}$ and $S_{L,1}^{(1)}$ are mean and linearized flame speed, $\Lambda (= T_2/T_1)$ is a temperature ratio of medium 2 to medium 1, and γ is specific heat ratio. Mass burning rate $m = \rho_1 S_L^{(1)}$ can be linearized to yield $S_{L,1}^{(1)}/S_{L,0}^{(1)} = m_1/m_0 - p_1^{(1)}/(\gamma p_0)$, where $p_1^{(1)}/\rho_{1,1} = c_1^2 = \gamma p_0/\rho_{1,0}$ is used. Then (2.7) can be rewritten in terms of m_1/m_0 and $p_1 = p_1^{(1)} = p_1^{(2)} + O(M_S^2)$.

$$\frac{v_{1,n}^{(2)}(t)}{c_1} - \frac{v_{1,n}^{(1)}(t)}{c_1} = (\Lambda - 1) M_S \left(\frac{m_1(t)}{m_0} - \frac{p_1(t)}{p_0} \right) + O(M_S^2), \quad (2.8)$$

where $m_1(t)/m_0$ can be further evaluated by linearizing the burning rate $M(v)$ ($\equiv m(t)/M_r$ where $M_r = (\rho S_L)_r$ is reference mass flux per unit area, $v = (\theta t_r)^{-1} t$ where θ is dimensionless activation energy, $t_r = \rho_r \lambda_r / c_{pr} M_r^2 = (\alpha_{th}/S_L^2)_r$ is a reference value of flame's diffusion time. The term 'diffusion' originates from the reasoning that t_r is a quantity associated with the thermal diffusivity α_{th} .) as reported by Peters & Ludford (1983, equation (22)).

$$b \frac{d \ln M(v)}{dv} - M^2(v) \{ \ln M^2(v) + \alpha (1 - \mathcal{P}(v)^{(\gamma-1)/\gamma}) \} = -2 \frac{\gamma - 1}{\gamma} \frac{d \ln \mathcal{P}(v)}{dv}, \quad (2.9)$$

where $\alpha = 2$, $b = 1 - Le^{-1}$, $\mathcal{P}(v) = p(t)/p_r$ with Le for Lewis number and p_r for reference pressure. Expanding M and \mathcal{P} in power series of θ^{-1} , i.e. $M = 1 + \theta^{-1} M_1 + O(\theta^{-2})$ and $\mathcal{P} = 1 + \theta^{-1} \mathcal{P}_1 + O(\theta^{-2})$, and collecting $O(\theta^{-1})$ in (2.9) yields a linearized mass burning rate with $M_r = m_0$ and $p_r = p_0$ for unity Lewis number.

$$\frac{m_1(t)}{m_0} = \frac{\gamma - 1}{\gamma p_0} \left(\frac{\alpha}{2} p_1(t) + \theta t_r \frac{\partial p_1(t)}{\partial t} \right) \quad (2.10)$$

which is then substituted into (2.8) to yield the acoustic velocity jump across a flame front of the order of $O(M_S)$ in terms of velocity potential.

$$\left(\frac{\partial \psi_c^{(2)}(\mathbf{R}, t)}{\partial n} - \frac{\partial \psi_c^{(1)}(\mathbf{R}, t)}{\partial n} + \beta_X \frac{\partial \psi_c^{(2)}(\mathbf{R}, t)}{\partial t} + \beta_Y \frac{\partial^2 \psi_c^{(2)}(\mathbf{R}, t)}{\partial t^2} \right)_{z=h(\mathbf{r}, t)} = 0, \quad (2.11)$$

where $\beta_X = (\Lambda - 1)/(c_2 \Lambda^{1/2})(\alpha/2(\gamma - 1) - \gamma)M_S$, $\beta_Y = (\Lambda - 1)(\gamma - 1)t_r \theta / (c_2 \Lambda^{1/2})M_S$.

Since the normal velocity in (2.11) is $\partial \psi / \partial n = \mathbf{n} \cdot \nabla \psi$ where \mathbf{n} is normal to the flame surface $G = z - h(\mathbf{r}, t) = 0$, i.e.

$$\mathbf{n} = \nabla G / |\nabla G| = (1 + |\nabla h|^2)^{-1/2}(\mathbf{e}_z - \nabla h), \quad (2.12)$$

then (2.11) is led further to the form

$$\begin{aligned} & (1 + |\nabla h|^2)^{-1/2} \left(\frac{\partial}{\partial z} - \nabla h \cdot \nabla \right) \psi_c^{(1)}(\mathbf{R}, t)|_{z=h(\mathbf{r}, t)} \\ & = \left[(1 + |\nabla h|^2)^{-1/2} \left(\frac{\partial}{\partial z} - \nabla h \cdot \nabla \right) - \beta_X \frac{\partial}{\partial t} - \beta_Y \frac{\partial^2}{\partial t^2} \right] \psi_c^{(2)}(\mathbf{R}, t)|_{z=h(\mathbf{r}, t)}. \end{aligned} \quad (2.13)$$

2.3. Evaluation of the scattering amplitudes using SPM

The pressure continuity in (2.6) and the velocity jump in (2.13) are expressed as the following forms using (2.4) and (2.5):

Pressure continuity:

$$\begin{aligned} & \rho_1 \left[\omega_0 (\rho_1 q_0^{(1)})^{-1/2} e^{i(\mathbf{k}_0 \cdot \mathbf{r} + q_0^{(1)} h(\mathbf{r}, t) - \omega_0 t)} \right. \\ & \quad \left. + \int_{\omega} \int_{\mathbf{k}} \int \omega S^{11}(\mathbf{k}, \mathbf{k}_0, \omega, \omega_0) (\rho_1 q_k^{(1)})^{-1/2} e^{i(\mathbf{k} \cdot \mathbf{r} - q_k^{(1)} h(\mathbf{r}, t) - \omega t)} d\mathbf{k} d\omega \right] \\ & = \rho_2 \int_{\omega} \int_{\mathbf{k}} \int \omega S^{21}(\mathbf{k}, \mathbf{k}_0, \omega, \omega_0) (\rho_2 q_k^{(2)})^{-1/2} e^{i(\mathbf{k} \cdot \mathbf{r} + q_k^{(2)} h(\mathbf{r}, t) - \omega t)} d\mathbf{k} d\omega \end{aligned} \quad (2.14)$$

Velocity jump:

$$\begin{aligned} & (1 + |\nabla h|^2)^{-1/2} (\rho_1 q_0^{(1)})^{-1/2} (q_0^{(1)} - \nabla h(\mathbf{r}, t) \cdot \mathbf{k}_0) e^{i(\mathbf{k}_0 \cdot \mathbf{r} + q_0^{(1)} h(\mathbf{r}, t) - \omega_0 t)} - (1 + |\nabla h|^2)^{-1/2} \\ & \quad \times \int_{\omega} \int_{\mathbf{k}} \int S^{11}(\mathbf{k}, \mathbf{k}_0, \omega, \omega_0) (\rho_1 q_k^{(1)})^{-1/2} (q_k^{(1)} + \nabla h(\mathbf{r}, t) \cdot \mathbf{k}) e^{i(\mathbf{k} \cdot \mathbf{r} - q_k^{(1)} h(\mathbf{r}, t) - \omega t)} d\mathbf{k} d\omega \\ & = \int_{\omega} \int_{\mathbf{k}} \int S^{21}(\mathbf{k}, \mathbf{k}_0, \omega, \omega_0) (\rho_2 q_k^{(2)})^{-1/2} \times \\ & \quad \left[(1 + |\nabla h|^2)^{-1/2} (q_k^{(2)} - \nabla h(\mathbf{r}, t) \cdot \mathbf{k}) + \beta_X \omega - i\beta_Y \omega^2 \right] e^{i(\mathbf{k} \cdot \mathbf{r} + q_k^{(2)} h(\mathbf{r}, t) - \omega t)} d\mathbf{k} d\omega. \end{aligned} \quad (2.15)$$

An approximate solution for the scattering amplitudes S^{11} and S^{21} in (2.14) and (2.15) can be obtained by using perturbation method, i.e. by expanding the scattering amplitudes in powers of h .

$$S^{N_1 N_2} = S_0^{N_1 N_2} + S_1^{N_1 N_2} + S_2^{N_1 N_2} + O(h^3), \quad (2.16)$$

where $S_n^{N_1 N_2} \sim O(h^n)$. Substituting (2.16) into (2.14) and (2.15) yields

$$\begin{aligned} & \rho_1 \left[\omega_0 (\rho_1 q_0^{(1)})^{-1/2} e^{i(\mathbf{k}_0 \cdot \mathbf{r} - \omega_0 t)} \left\{ 1 + i q_0^{(1)} h(\mathbf{r}, t) - \frac{1}{2} (q_0^{(1)} h(\mathbf{r}, t))^2 + O(h^3) \right\} \right. \\ & \quad \left. + \int_{\omega} \int_{\mathbf{k}} \int \omega (S_0^{11} + S_1^{11} + S_2^{11} + O(h^3)) (\rho_1 q_k^{(1)})^{-1/2} e^{i(\mathbf{k} \cdot \mathbf{r} - \omega t)} \right. \end{aligned}$$

$$\begin{aligned}
& \times \left\{ 1 - iq_k^{(1)}h(\mathbf{r}, t) - \frac{1}{2}(q_k^{(1)}h(\mathbf{r}, t))^2 + O(h^3) \right\} d\mathbf{k} d\omega \Big] \\
= & \rho_2 \int_{\omega} \int_{\mathbf{k}} \int \omega (S_0^{21} + S_1^{21} + S_2^{21} + O(h^3)) (\rho_2 q_k^{(2)})^{-1/2} e^{i(\mathbf{k} \cdot \mathbf{r} - \omega t)} \\
& \times \left\{ 1 + iq_k^{(2)}h(\mathbf{r}, t) - \frac{1}{2}(q_k^{(2)}h(\mathbf{r}, t))^2 + O(h^3) \right\} d\mathbf{k} d\omega, \tag{2.17} \\
& \left(1 - \frac{1}{2} |\nabla h|^2 + O(h^4) \right) (\rho_1 q_0^{(1)})^{-1/2} (q_0^{(1)} - \nabla h(\mathbf{r}, t) \cdot \mathbf{k}_0) \\
& \times \left\{ 1 + iq_0^{(1)}h(\mathbf{r}, t) - \frac{1}{2}(q_0^{(1)}h(\mathbf{r}, t))^2 + O(h^3) \right\} e^{i(\mathbf{k}_0 \cdot \mathbf{r} - \omega_0 t)} \\
& - \int_{\omega} \int_{\mathbf{k}} \int \left(1 - \frac{1}{2} |\nabla h|^2 + O(h^4) \right) (S_0^{11} + S_1^{11} + S_2^{11} + O(h^3)) (\rho_1 q_k^{(1)})^{-1/2} \\
& \times (q_k^{(1)} + \nabla h(\mathbf{r}, t) \cdot \mathbf{k}) \left\{ 1 - iq_k^{(1)}h(\mathbf{r}, t) - \frac{1}{2}(q_k^{(1)}h(\mathbf{r}, t))^2 + O(h^3) \right\} e^{i(\mathbf{k} \cdot \mathbf{r} - \omega t)} d\mathbf{k} d\omega \\
= & \int_{\omega} \int_{\mathbf{k}} \int (S_0^{21} + S_1^{21} + S_2^{21} + O(h^3)) (\rho_2 q_k^{(2)})^{-1/2} \\
& \times \left[\left(1 - \frac{1}{2} |\nabla h|^2 + O(h^4) \right) (q_k^{(2)} - \nabla h(\mathbf{r}, t) \cdot \mathbf{k}) + \beta(\omega) \right] \\
& \times \left\{ 1 + iq_k^{(2)}h(\mathbf{r}, t) - \frac{1}{2}(q_k^{(2)}h(\mathbf{r}, t))^2 + O(h^3) \right\} e^{i(\mathbf{k} \cdot \mathbf{r} - \omega t)} d\mathbf{k} d\omega \tag{2.18}
\end{aligned}$$

where $(1 + |\nabla h|^2)^{-1/2} = 1 - |\nabla h|^2/2 + O(h^4)$ is used and $\exp(iq_k h(\mathbf{r}, t))$ terms are expanded in a Taylor series by assuming a small *Rayleigh parameter* and a small slope

$$q_k h(\mathbf{r}, t) \ll 1, \quad \nabla h(\mathbf{r}, t) \cdot \mathbf{k} / q_k \ll 1, \tag{2.19}$$

where the second one imposes the condition that the slope of surface roughness be smaller than the grazing angle of all incident and scattered waves. Equation (2.19) can also be written in statistical forms in cases where random oscillations are present.

$$\tilde{\sigma} \cos \phi \ll 1 \quad (\text{small r.m.s. height}), \quad \tilde{\sigma}_{\Delta} \tan \phi \ll 1 \quad (\text{small slope}), \tag{2.20}$$

where $\tilde{\sigma} = K_0 \sigma$ ($K_0 = \omega_0 / c_1$, $\sigma = \langle h^2 \rangle^{1/2}$) is a non-dimensional r.m.s. height of a flame front, and $\tilde{\sigma}_{\Delta} = \sqrt{2} \sigma / l_c$ is the r.m.s. gradient (Ogilvy 1991, p. 22), and ϕ is a polar angle of the incident wave. By assuming that $\tilde{\sigma} \cos \phi \leq 0.3$, a maximum frequency below which the present analysis applies is obtained by $f_{max} = Kc / 2\pi \approx 540$ Hz for normal incidence ($\phi = 0^\circ$) with $\sigma = 3$ cm, $c = 340$ ms⁻¹. (Note that an r.m.s. flame height of 3 cm represents a turbulent flame with a peak to peak amplitude of about $2\sqrt{2}\sigma \approx 9$ cm.) This frequency range covers a considerable part of instability frequencies that are often observed in typical gas turbine combustors (Lieuwen & Yang 2005). Collecting the terms of $O(h^0)$ in (2.17) and (2.18), multiplying $\exp[-i(\mathbf{k}' \cdot \mathbf{r} - \omega' t)] / (2\pi)^3$, and integrating with respect to \mathbf{r} and t yields the zeroth order scattering

amplitudes (Cho 2006).

$$S_0^{11}(\mathbf{k}, \mathbf{k}_0, \omega, \omega_0) = R(\mathbf{k}, \omega)\delta(\mathbf{k} - \mathbf{k}_0)\delta(\omega - \omega_0), R(\mathbf{k}, \omega) = \frac{\rho_2 q_k^{(1)} - \rho_1 (q_k^{(2)} + \beta(\omega))}{\rho_2 q_k^{(1)} + \rho_1 (q_k^{(2)} + \beta(\omega))} \quad (2.21)$$

$$S_0^{21}(\mathbf{k}, \mathbf{k}_0, \omega, \omega_0) = D(\mathbf{k}, \omega)\delta(\mathbf{k} - \mathbf{k}_0)\delta(\omega - \omega_0), D(\mathbf{k}, \omega) = \frac{2(\rho_1 \rho_2 q_k^{(1)} q_k^{(2)})^{1/2}}{\rho_2 q_k^{(1)} + \rho_1 (q_k^{(2)} + \beta(\omega))}, \quad (2.22)$$

where $\beta(\omega) = \beta_X \omega - i\beta_Y \omega^2$ is a *jump factor* in acoustic velocity across a flame and δ is dirac delta function. R and D denote the reflection and transmission coefficient, respectively, from the mean flat surface. Note that the energy conservation relationship, $R^2 + D^2 = 1$, holds in case of no jump condition ($\beta = 0$); i.e. the sum of the reflected and transmitted energies from the mean surface is equal to the incident energy. Similarly, collecting the terms of $O(h^1)$ in (2.17) and (2.18) leads to the solution of the first-order scattering amplitudes after some manipulations (Cho 2006).

$$S_1^{11}(\mathbf{k}, \mathbf{k}_0, \omega, \omega_0) = A(\mathbf{k}, \mathbf{k}_0, \omega, \omega_0)h(\mathbf{k} - \mathbf{k}_0, \omega - \omega_0) \quad (2.23)$$

$$S_1^{21}(\mathbf{k}, \mathbf{k}_0, \omega, \omega_0) = B(\mathbf{k}, \mathbf{k}_0, \omega, \omega_0)h(\mathbf{k} - \mathbf{k}_0, \omega - \omega_0) \quad (2.24)$$

$$A(\mathbf{k}, \mathbf{k}_0, \omega, \omega_0) = \frac{2i(q_0^{(1)} q_k^{(1)})^{1/2}}{[\rho_2 q_0^{(1)} + \rho_1 (q_0^{(2)} + \beta(\omega_0))] [\rho_2 q_k^{(1)} + \rho_1 (q_k^{(2)} + \beta(\omega))]} \times \left[\frac{\omega_0}{\omega} \rho_1 (q_k^{(2)} + \beta(\omega)) \{(\rho_2 - \rho_1)q_0^{(2)} - \rho_1 \beta(\omega_0)\} + \rho_2 \alpha(\mathbf{k}, \mathbf{k}_0, \omega_0) \right] \quad (2.25)$$

$$B(\mathbf{k}, \mathbf{k}_0, \omega, \omega_0) = \frac{2i(\rho_1 \rho_2 q_0^{(1)} q_k^{(2)})^{1/2}}{[\rho_2 q_0^{(1)} + \rho_1 (q_0^{(2)} + \beta(\omega_0))] [\rho_2 q_k^{(1)} + \rho_1 (q_k^{(2)} + \beta(\omega))]} \times \left[-\frac{\omega_0}{\omega} q_k^{(1)} \{(\rho_2 - \rho_1)q_0^{(2)} - \rho_1 \beta(\omega_0)\} + \alpha(\mathbf{k}, \mathbf{k}_0, \omega_0) \right] \quad (2.26)$$

$$\alpha(\mathbf{k}, \mathbf{k}_0, \omega_0) = \rho_2 \left\{ \left(\frac{\omega_0}{c_1} \right)^2 - \mathbf{k} \cdot \mathbf{k}_0 \right\} - \rho_1 \left\{ \left(\frac{\omega_0}{c_2} \right)^2 - \mathbf{k} \cdot \mathbf{k}_0 + q_0^{(2)} \beta(\omega_0) \right\} \quad (2.27)$$

$$h(\mathbf{k}, \omega) = \frac{1}{(2\pi)^3} \int_r \int_t h(\mathbf{r}, t) e^{-i(\mathbf{k} \cdot \mathbf{r} - \omega t)} dt d\mathbf{r}. \quad (2.28)$$

Equations (2.23)–(2.27) coincide with the formulae of the scattering amplitudes that are derived by Voronovich (1999) for a stationary surface ($\omega = \omega_0$) with no jump condition in acoustic velocity ($\beta = 0$). The second-order solutions of the scattering amplitudes can be obtained by collecting the terms of $O(h^2)$ in (2.17) and (2.18) (see Cho 2006 for details). Note that the second-order scattering amplitudes play a key role in demonstrating the acoustic energy balance that accounts for coherent energy damping which is transmitted to incoherent energy production (see (2.48)

for details).

$$\left. \begin{aligned} \{S_2^{11}(\mathbf{k}, \mathbf{k}_0, \omega, \omega_0)\} \\ \{S_2^{21}(\mathbf{k}, \mathbf{k}_0, \omega, \omega_0)\} \end{aligned} \right\} = \frac{(\rho_1 \rho_2 q_k^{(1)} q_k^{(2)})^{1/2}}{\rho_2 q_k^{(1)} + \rho_1 (q_k^{(2)} + \beta(\omega))} \times \left\{ \begin{aligned} \int_{\omega'} \int_{\mathbf{k}'} \int F(\mathbf{k}', \mathbf{k}_0, \mathbf{k}, \omega', \omega_0, \omega) h(\mathbf{k} - \mathbf{k}', \omega - \omega') h(\mathbf{k}' - \mathbf{k}_0, \omega' - \omega_0) d\mathbf{k}' d\omega' \\ \int_{\omega'} \int_{\mathbf{k}'} \int G(\mathbf{k}', \mathbf{k}_0, \mathbf{k}, \omega', \omega_0, \omega) h(\mathbf{k} - \mathbf{k}', \omega - \omega') h(\mathbf{k}' - \mathbf{k}_0, \omega' - \omega_0) d\mathbf{k}' d\omega' \end{aligned} \right\} \quad (2.29)$$

$$\begin{aligned} F(\mathbf{k}', \mathbf{k}_0, \mathbf{k}, \omega', \omega_0, \omega) &= \frac{(\rho_1 \rho_2 q_0^{(1)} / q_k^{(2)})^{1/2}}{\rho_2 q_0^{(1)} + \rho_1 (q_0^{(2)} + \beta(\omega_0))} \\ &\times \left\{ \left[\left(\frac{\omega_0}{c_1} \right)^2 - \left(\frac{\omega_0}{c_2} \right)^2 \right] \left[\frac{\omega_0}{\omega} (q_k^{(2)} + \beta(\omega)) \right. \right. \\ &\left. \left. - (q_0^{(2)} + \beta(\omega_0)) \right] + \beta(\omega_0) [\mathbf{k}' \cdot (\mathbf{k} - \mathbf{k}') + \mathbf{k}_0 \cdot (\mathbf{k}' - \mathbf{k}_0)] \right\} \\ &+ \frac{i}{(q_k^{(2)})^{1/2}} \left\{ \frac{\omega'}{\omega} \left(\frac{\rho_1 q_{k'}^{(1)}}{\rho_2} \right)^{1/2} (q_k^{(2)} + \beta(\omega)) \right. \\ &+ \left. \left(\frac{\rho_2}{\rho_1 q_{k'}^{(1)}} \right)^{1/2} \left[\left(\frac{\omega'}{c_1} \right)^2 - \mathbf{k}' \cdot \mathbf{k} \right] \right\} A(\mathbf{k}', \mathbf{k}_0, \omega', \omega_0) \\ &+ \frac{i}{(q_k^{(2)})^{1/2}} \left\{ \frac{\omega'}{\omega} (q_{k'}^{(2)})^{1/2} (q_k^{(2)} + \beta(\omega)) \right. \\ &\left. - (q_{k'}^{(2)})^{-1/2} \left[\left(\frac{\omega'}{c_2} \right)^2 - \mathbf{k}' \cdot \mathbf{k} + \beta(\omega') q_{k'}^{(2)} \right] \right\} B(\mathbf{k}', \mathbf{k}_0, \omega', \omega_0), \quad (2.30) \end{aligned}$$

$$\begin{aligned} G(\mathbf{k}', \mathbf{k}_0, \mathbf{k}, \omega', \omega_0, \omega) &= \frac{-(q_0^{(1)} / q_k^{(1)})^{1/2}}{\rho_2 q_0^{(1)} + \rho_1 (q_0^{(2)} + \beta(\omega_0))} \left\{ \left[\left(\frac{\omega_0}{c_1} \right)^2 - \left(\frac{\omega_0}{c_2} \right)^2 \right] \right. \\ &\times \left. \left[\frac{\omega_0}{\omega} \rho_2 q_k^{(1)} + \rho_1 (q_0^{(2)} + \beta(\omega_0)) \right] - \rho_1 \beta(\omega_0) [\mathbf{k}' \cdot (\mathbf{k} - \mathbf{k}') + \mathbf{k}_0 \cdot (\mathbf{k}' - \mathbf{k}_0)] \right\} \\ &+ i \left\{ -\frac{\omega'}{\omega} (q_k^{(1)} q_{k'}^{(1)})^{1/2} + (q_k^{(1)} q_{k'}^{(1)})^{-1/2} \left[\left(\frac{\omega'}{c_1} \right)^2 - \mathbf{k}' \cdot \mathbf{k} \right] \right\} A(\mathbf{k}', \mathbf{k}_0, \omega', \omega_0) \\ &- i \left\{ \frac{\omega'}{\omega} \left(\frac{\rho_2}{\rho_1} q_k^{(1)} q_{k'}^{(2)} \right)^{1/2} + \left(\frac{\rho_2}{\rho_1} q_k^{(1)} q_{k'}^{(2)} \right)^{-1/2} \left[\left(\frac{\omega'}{c_2} \right)^2 - \mathbf{k}' \cdot \mathbf{k} + \beta(\omega') q_{k'}^{(2)} \right] \right\} B(\mathbf{k}', \mathbf{k}_0, \omega', \omega_0). \quad (2.31) \end{aligned}$$

From (2.21)–(2.24) and (2.29), the scattering amplitudes with an accuracy of the second order of flame height can now be written as

$$\begin{aligned} S^{11}(\mathbf{k}, \mathbf{k}_0, \omega, \omega_0) &= \sum_{n=0}^2 S_n^{11}(\mathbf{k}, \mathbf{k}_0, \omega, \omega_0) + O(h^3) \\ &= R(\mathbf{k}, \omega) \delta(\mathbf{k} - \mathbf{k}_0) \delta(\omega - \omega_0) + A(\mathbf{k}, \mathbf{k}_0, \omega, \omega_0) h(\mathbf{k} - \mathbf{k}_0, \omega - \omega_0) \\ &\quad + \frac{1}{2} D(\mathbf{k}, \omega) \int_{\omega'} \int_{\mathbf{k}'} \int F(\mathbf{k}', \mathbf{k}_0, \mathbf{k}, \omega', \omega_0, \omega) h(\mathbf{k} - \mathbf{k}', \omega - \omega') \\ &\quad \times h(\mathbf{k}' - \mathbf{k}_0, \omega' - \omega_0) d\mathbf{k}' d\omega' \quad (2.32) \end{aligned}$$

$$\begin{aligned}
 S^{21}(\mathbf{k}, \mathbf{k}_0, \omega, \omega_0) &= \sum_{n=0}^2 S_n^{21}(\mathbf{k}, \mathbf{k}_0, \omega, \omega_0) + O(h^3) \\
 &= D(\mathbf{k}, \omega)\delta(\mathbf{k} - \mathbf{k}_0)\delta(\omega - \omega_0) + B(\mathbf{k}, \mathbf{k}_0, \omega, \omega_0)h(\mathbf{k} - \mathbf{k}_0, \omega - \omega_0) \\
 &\quad + \frac{1}{2}D(\mathbf{k}, \omega) \int_{\omega'} \int_{\mathbf{k}'} \int G(\mathbf{k}', \mathbf{k}_0, \mathbf{k}, \omega', \omega_0, \omega)h(\mathbf{k} - \mathbf{k}', \omega - \omega') \\
 &\quad \times h(\mathbf{k}' - \mathbf{k}_0, \omega' - \omega_0)d\mathbf{k}'d\omega'. \tag{2.33}
 \end{aligned}$$

2.4. Coherent and incoherent fields

Scattering from a randomly rough surface consists of coherent part which propagates in the specular direction and incoherent part which propagates in *off-specular* (diffuse) directions. Coherent field has constant and predictable phase relationship with an incident wave while incoherent field has no fixed phase relationship with an incident wave (Ogilvy 1991). Due to such random phase relationship of incoherent field, taking an ensemble average of scattered fields eliminates incoherent part and, therefore, yields mean scattered acoustic field which is coherent. For instance, taking an ensemble average of the scattering amplitudes in (2.32) and (2.33) yields the mean reflection and transmission quantities of scattered acoustic fields.

$$\langle S^{11}(\mathbf{k}, \mathbf{k}_0, \omega, \omega_0) \rangle = \langle V(\mathbf{k}, \omega) \rangle \delta(\mathbf{k} - \mathbf{k}_0)\delta(\omega - \omega_0), \tag{2.34}$$

$$\langle S^{21}(\mathbf{k}, \mathbf{k}_0, \omega, \omega_0) \rangle = \langle T(\mathbf{k}, \omega) \rangle \delta(\mathbf{k} - \mathbf{k}_0)\delta(\omega - \omega_0), \tag{2.35}$$

where the mean reflection and transmission coefficients are expressed as

$$\langle V(\mathbf{k}, \omega) \rangle = R(\mathbf{k}, \omega) + \frac{1}{2}D(\mathbf{k}, \omega) \int_{\omega'} \int_{\mathbf{k}'} \int F(\mathbf{k}', \mathbf{k}_0, \mathbf{k}, \omega', \omega_0, \omega)W(\mathbf{k} - \mathbf{k}', \omega - \omega') d\mathbf{k}' d\omega' \tag{2.36}$$

$$\langle T(\mathbf{k}, \omega) \rangle = D(\mathbf{k}, \omega) \left[1 + \frac{1}{2} \int_{\omega'} \int_{\mathbf{k}'} \int G(\mathbf{k}', \mathbf{k}_0, \mathbf{k}, \omega', \omega_0, \omega)W(\mathbf{k} - \mathbf{k}', \omega - \omega') d\mathbf{k}' d\omega' \right]. \tag{2.37}$$

Equations (2.34) and (2.35) imply that the mean scattering waves propagate in the specular direction, $\mathbf{k} = \mathbf{k}_0$, with the incident wave frequency, $\omega = \omega_0$. Note in (2.36) and (2.37) that the mean scattering coefficients $\langle V \rangle$ and $\langle T \rangle$ differ from the reflection and transmission coefficients from the mean plane surface, R and D , by the second-order terms. These second-order terms account for coherent energy damping due to surface roughness. On the other hand, the incoherent field can be obtained by estimating the *second moment* of the scattering amplitudes $\langle \Delta S^{11} \Delta S^{11} \rangle$ (ΔS^{11} is the fluctuation in the scattering amplitude), which describes incoherent energy production (see §3 for detailed analysis). W in (2.36) is the power spectral density of flame front height, which is defined as Fourier transform of the correlation function of flame front height (Meirovitch 1971, p. 490). Note that W is related to flame height statistics in the form

$$\langle h(\mathbf{k}_1, \omega_1)h(\mathbf{k}_2, \omega_2) \rangle = W(\mathbf{k}_1, \omega_1)\delta(\mathbf{k}_1 + \mathbf{k}_2)\delta(\omega_1 + \omega_2) \tag{2.38}$$

which is an extended version of that in Voronovich (1999, p. 80) and can be proved by using the correlation function $\tilde{W}(\boldsymbol{\xi}, \eta)$ ($\boldsymbol{\xi} = \mathbf{r}_1 - \mathbf{r}_2$, $\eta = t_1 - t_2$), which is a function

of ξ and η only in case of spatially homogeneous and temporally stationary statistics.

$$\begin{aligned}
\bar{W}(\xi, \eta) &= \langle h(\mathbf{r}_1, t_1)h(\mathbf{r}_2, t_2) \rangle \\
&= \left\langle \int_{\mathbf{k}_1} \int_{\omega_1} \int h(\mathbf{k}_1, \omega_1) e^{i(\mathbf{k}_1 \cdot \mathbf{r}_1 - \omega_1 t_1)} d\omega_1 d\mathbf{k}_1 \times \int_{\mathbf{k}_2} \int_{\omega_2} \int h(\mathbf{k}_2, \omega_2) e^{i(\mathbf{k}_2 \cdot \mathbf{r}_2 - \omega_2 t_2)} d\omega_2 d\mathbf{k}_2 \right\rangle \\
&= \int_{\mathbf{k}_1} \int_{\omega_1} \int_{\mathbf{k}_2} \int_{\omega_2} \langle h(\mathbf{k}_1, \omega_1)h(\mathbf{k}_2, \omega_2) \rangle e^{i[\mathbf{k}_1 \cdot \xi - \omega_1 \eta + (\mathbf{k}_1 + \mathbf{k}_2) \cdot \mathbf{r}_2 - (\omega_1 + \omega_2)t_2]} d\omega_2 d\mathbf{k}_2 d\omega_1 d\mathbf{k}_1,
\end{aligned} \tag{2.39}$$

where $(\mathbf{k}_1 + \mathbf{k}_2) \cdot \mathbf{r}_2 - (\omega_1 + \omega_2)t_2$ in the exponential term should vanish in order for $\bar{W}(\xi, \eta)$ to be a function of ξ and η only. This implies that $\langle h(\mathbf{k}_1, \omega_1)h(\mathbf{k}_2, \omega_2) \rangle$ should vanish unless $\mathbf{k}_1 + \mathbf{k}_2 = 0$ and $\omega_1 + \omega_2 = 0$, which leads to (2.38) by comparing (2.39) with $\bar{W}(\xi, \eta) = \int_{\mathbf{k}_1} \int_{\omega_1} W(\mathbf{k}_1, \omega_1) e^{i(\mathbf{k}_1 \cdot \xi - \omega_1 \eta)} d\omega_1 d\mathbf{k}_1$. In case of pressure release condition ($\rho_2/\rho_1 \rightarrow 0$) at a stationary surface ($\omega = \omega_0$) with no velocity jump ($\beta = 0$), the mean reflection coefficient in (2.36) is reduced to the form

$$\langle V(\mathbf{k}_0, \omega_0) \rangle_{\beta=0} = -1 + 2q_0^{(1)} \int_{\mathbf{k}'} \int q_{\mathbf{k}'}^{(1)} W(\mathbf{k}_0 - \mathbf{k}') d\mathbf{k}' \tag{2.40}$$

which is equivalent to the expression from Voronovich (1999, p. 80).

2.5. Formulation of the scattered acoustic energy budget

An averaged acoustic energy of scattered waves can be evaluated from (A 6) (see appendix A). Comparing (A 4) with the reflected acoustic pressure and velocity fields in (2.2)–(2.4) yields the complex amplitudes of acoustic pressure and velocity

$$P(\mathbf{k}, \omega, z) = \frac{\omega}{\omega_0} \left(\frac{q_0^{(1)}}{q_{\mathbf{k}}^{(1)}} \right)^{1/2} S^{11}(\mathbf{k}, \mathbf{k}_0, \omega, \omega_0) e^{-iq_{\mathbf{k}}^{(1)} z}$$

$$V(\mathbf{k}, \omega, z) = \frac{\varepsilon c_1}{\omega_0} \left(\frac{q_0^{(1)}}{q_{\mathbf{k}}^{(1)}} \right)^{1/2} S^{11}(\mathbf{k}, \mathbf{k}_0, \omega, \omega_0) \mathbf{K}_-^{(1)} e^{-iq_{\mathbf{k}}^{(1)} z} (\varepsilon = |P_I|/(\rho_1 c_1^2), \mathbf{K}_-^{(1)} = (k_x, k_y, -q_{\mathbf{k}}^{(1)})) \tag{2.41}$$

which are substituted into (A 6) to yield the ensemble-averaged energy flux using the correlation function of the scattering amplitudes.

$$\begin{aligned}
&\langle S^{11}(\mathbf{k}, \mathbf{k}_0, \omega, \omega_0) S^{11}(-\mathbf{k}', \mathbf{k}_0, -\omega', \omega_0) \rangle \\
&= \langle S_{(\mathbf{k}, \mathbf{k}_0, \omega, \omega_0)}^{11} \rangle \langle S_{(-\mathbf{k}', \mathbf{k}_0, -\omega', \omega_0)}^{11} \rangle + \langle \Delta S_{(\mathbf{k}, \mathbf{k}_0, \omega, \omega_0)}^{11} \Delta S_{(-\mathbf{k}', \mathbf{k}_0, -\omega', \omega_0)}^{11} \rangle \\
&= \langle V(\mathbf{k}, \omega) \rangle \langle V(-\mathbf{k}', -\omega') \rangle \delta(\mathbf{k} - \mathbf{k}_0) \delta(\omega - \omega_0) \delta(\mathbf{k}' + \mathbf{k}_0) \delta(\omega' + \omega_0) \\
&\quad + A(\mathbf{k}, \mathbf{k}_0, \omega, \omega_0) A(-\mathbf{k}', \mathbf{k}_0, -\omega', \omega_0) W(\mathbf{k} - \mathbf{k}_0, \omega - \omega_0) \delta(\mathbf{k} - \mathbf{k}' - 2\mathbf{k}_0) \\
&\quad \times \delta(\omega - \omega' - 2\omega_0) + O(h^3),
\end{aligned} \tag{2.42}$$

$$\begin{aligned}
&\langle S^{11}(\mathbf{k}, \mathbf{k}_0, \omega, \omega_0) S^{11*}(\mathbf{k}', \mathbf{k}_0, \omega', \omega_0) \rangle \\
&= \langle V(\mathbf{k}, \omega) \rangle \langle V^*(\mathbf{k}', \omega') \rangle \delta(\mathbf{k} - \mathbf{k}_0) \delta(\omega - \omega_0) \delta(\mathbf{k}' - \mathbf{k}_0) \delta(\omega' - \omega_0) \\
&\quad + A(\mathbf{k}, \mathbf{k}_0, \omega, \omega_0) A^*(\mathbf{k}', \mathbf{k}_0, \omega', \omega_0) W(\mathbf{k} - \mathbf{k}_0, \omega - \omega_0) \delta(\mathbf{k} - \mathbf{k}') \\
&\quad \times \delta(\omega - \omega') + O(h^3),
\end{aligned} \tag{2.43}$$

where the fluctuation in the scattering amplitude

$$\begin{aligned}
\Delta S_{(\mathbf{k}, \mathbf{k}_0, \omega, \omega_0)}^{11} &= S^{11}(\mathbf{k}, \mathbf{k}_0, \omega, \omega_0) - \langle S^{11}(\mathbf{k}, \mathbf{k}_0, \omega, \omega_0) \rangle \\
&= A(\mathbf{k}, \mathbf{k}_0, \omega, \omega_0) h(\mathbf{k} - \mathbf{k}_0, \omega - \omega_0) + O(h^2)
\end{aligned} \tag{2.44}$$

was used together with (2.38) and $h^*(\mathbf{k}, \omega) = h(-\mathbf{k}, -\omega)$ (superscript * denotes the complex conjugate). Then the reflected energy in unit area of the mean flame surface normalized by the incident energy flux $\mathbf{I}_{av,I} \cdot \mathbf{n} (= \varepsilon c_1 q_0^{(1)} / (2\omega_0))$ can be obtained with an accuracy of $O(h^2)$ from (2.41)–(2.43) and (A 6).

$$E_R = \langle \mathbf{I}_{av} \rangle_R \cdot (-\mathbf{n}) / \mathbf{I}_{av,I} \cdot \mathbf{n} = |\langle V(\mathbf{k}_0, \omega_0) \rangle|^2 + \int_{\omega} \int_{|\mathbf{k}| < |\omega|/c_1} \int \sigma_R(\mathbf{k}, \mathbf{k}_0, \omega, \omega_0) d\mathbf{k} d\omega \quad (2.45)$$

where the first term represents coherent energy of the scattering waves reflected in the specular direction while the second term represents incoherent energy due to flame surface wrinkling. That incoherent energy takes on an integral form implying that the waves contributing to the incoherent energy are characterized by a broad range of propagation directions and frequencies. The integrand in the second term is *the reflected scattering cross-section* defined as $\sigma_R(\mathbf{k}, \mathbf{k}_0, \omega, \omega_0) = (\omega/\omega_0) |A(\mathbf{k}, \mathbf{k}_0, \omega, \omega_0)|^2 W(\mathbf{k} - \mathbf{k}_0, \omega - \omega_0)$. The transmitted acoustic energy can be evaluated in a similar manner to yield

$$E_T = \langle \mathbf{I}_{av} \rangle_T \cdot \mathbf{n} / \mathbf{I}_{av,I} \cdot \mathbf{n} = \frac{Re(q_0^{(2)})}{|q_0^{(2)}|} |\langle T(\mathbf{k}_0, \omega_0) \rangle|^2 + \int_{\omega} \int_{|\mathbf{k}| < |\omega|/c_2} \int \sigma_T(\mathbf{k}, \mathbf{k}_0, \omega, \omega_0) d\mathbf{k} d\omega, \quad (2.46)$$

where $\sigma_T(\mathbf{k}, \mathbf{k}_0, \omega, \omega_0) = (\omega/\omega_0) |B(\mathbf{k}, \mathbf{k}_0, \omega, \omega_0)|^2 W(\mathbf{k} - \mathbf{k}_0, \omega - \omega_0)$ is *the transmitted scattering cross-section*. Total acoustic energy after scattering can then be obtained by combining (2.45) and (2.46).

$$E_{total} = E_{co} + E_{inc} \quad (2.47)$$

where

$$\begin{aligned} E_{co} &= |\langle V(\mathbf{k}_0, \omega_0) \rangle|^2 + Re(q_0^{(2)} / |q_0^{(2)}|) |\langle T(\mathbf{k}_0, \omega_0) \rangle|^2 \\ &= |R(\mathbf{k}_0, \omega_0)|^2 + \frac{Re(q_0^{(2)})}{|q_0^{(2)}|} |D(\mathbf{k}_0, \omega_0)|^2 + \int_{\omega} \int_{\mathbf{k}} \int Re [H(\mathbf{k}, \mathbf{k}_0, \omega, \omega_0)] \\ &\quad \times W(\mathbf{k}_0 - \mathbf{k}, \omega_0 - \omega) d\mathbf{k} d\omega, \\ E_{inc} &= \int_{\omega} \int_{|\mathbf{k}| < |\omega|/c_1} \int \sigma_R(\mathbf{k}, \mathbf{k}_0, \omega, \omega_0) d\mathbf{k} d\omega + \int_{\omega} \int_{|\mathbf{k}| < |\omega|/c_2} \int \sigma_T(\mathbf{k}, \mathbf{k}_0, \omega, \omega_0) d\mathbf{k} d\omega. \end{aligned}$$

E_{co} and E_{inc} denote coherent and incoherent energies, and the H term is of the form

$$\begin{aligned} H(\mathbf{k}, \mathbf{k}_0, \omega, \omega_0) &= R^*(\mathbf{k}_0, \omega_0) D(\mathbf{k}_0, \omega_0) F(\mathbf{k}, \mathbf{k}_0, \mathbf{k}_0, \omega, \omega_0, \omega_0) \\ &\quad + Re(q_0^{(2)} / |q_0^{(2)}|) |D(\mathbf{k}_0, \omega_0)|^2 G(\mathbf{k}, \mathbf{k}_0, \mathbf{k}_0, \omega, \omega_0, \omega_0) \end{aligned}$$

which describes coherent energy damping that arises from the energy transfer from coherent to incoherent field due to flame surface wrinkling. Since acoustic energy is produced or damped either by the acoustic velocity jump due to unsteady heat release or by unsteady motion of flame, neglectation of these unsteady effects, i.e. $\beta = 0$ and $\omega = \omega_0$, should manifest the *acoustic energy balance*, which states that the scattered acoustic energy is equal to the original energy from incident waves. Some manipulation can in fact show that coherent energy damping (the H term in E_{co}) is the counterpart of incoherent energy production (the σ terms in E_{inc}) in (2.47) by

proving the following identities (Cho 2006):

$$\begin{aligned}
& - \operatorname{Re} [H(\mathbf{k}, \mathbf{k}_0, \omega_0, \omega_0)]_{\beta=0} \\
& = \operatorname{Re}(q_k^{(1)}/|q_k^{(1)}|) |A(\mathbf{k}, \mathbf{k}_0, \omega_0, \omega_0)|_{\beta=0}^2 + \operatorname{Re}(q_k^{(2)}/|q_k^{(2)}|) |B(\mathbf{k}, \mathbf{k}_0, \omega_0, \omega_0)|_{\beta=0}^2 \\
& = D^2(\mathbf{k}_0, \omega_0) \left\{ q_0^{(2)} \left(1 - \frac{\rho_1}{\rho_2}\right)^2 \operatorname{Re} \left[\frac{\rho_2 q_k^{(1)} q_k^{(2)}}{\rho_2 q_k^{(1)} + \rho_1 q_k^{(2)}} \right] + \frac{\alpha^2(\mathbf{k}, \mathbf{k}_0, \omega_0)}{\rho_1 q_0^{(2)}} \operatorname{Re} \left[\frac{1}{\rho_2 q_k^{(1)} + \rho_1 q_k^{(2)}} \right] \right\}_{\beta=0}, \tag{2.48}
\end{aligned}$$

where the last expression is non-negative, which implies the one-way energy transfer from coherent to incoherent field; i.e. incoherent energy is produced (positive) at the expense of coherent energy damping (negative) by a wrinkled surface if neither velocity jump nor unsteady surface motion is considered. Equation (2.48) leads (2.47) to the acoustic energy balance in case of no unsteady effects.

$$E_{total}|_{no-unsteady} = |R(\mathbf{k}_0, \omega_0)|_{\beta=0}^2 + |D(\mathbf{k}_0, \omega_0)|_{\beta=0}^2 = 1. \tag{2.49}$$

In case of pressure release condition ($\rho_2/\rho_1 \rightarrow 0$) with no unsteady effects, (2.47) can be expressed as the form by using $\langle T(\mathbf{k}_0, \omega_0) \rangle_{\beta=0} \rightarrow 0$

$$|\langle V(\mathbf{k}_0, \omega_0) \rangle|_{\beta=0}^2 + 4q_0^{(1)} \int \int_{|\mathbf{k}| < \omega_0/c_1} q_k^{(1)} W(\mathbf{k} - \mathbf{k}_0) d\mathbf{k} = 1 + O(h^3) \tag{2.50}$$

which is equivalent to the expression from Voronovich (1999, p. 81). *Net acoustic energy* after scattering can then be evaluated by

$$\Delta E = E_{total} - 1 = \Delta E_{co} + \Delta E_{inc} \tag{2.51}$$

$$\Delta E_{co} = |\langle V(\mathbf{k}_0, \omega_0) \rangle|^2 - |R(\mathbf{k}_0, \omega_0)|_{\beta=0}^2 + \operatorname{Re}(q_0^{(2)}/|q_0^{(2)}|) |\langle T(\mathbf{k}_0, \omega_0) \rangle|^2 - |D(\mathbf{k}_0, \omega_0)|_{\beta=0}^2 \tag{2.52}$$

$$\Delta E_{inc} = \int_{\omega} \int_{|\mathbf{k}| < |\omega|/c_1} \int \sigma_R(\mathbf{k}, \mathbf{k}_0, \omega, \omega_0) d\mathbf{k} d\omega + \int_{\omega} \int_{|\mathbf{k}| < |\omega|/c_2} \int \sigma_T(\mathbf{k}, \mathbf{k}_0, \omega, \omega_0) d\mathbf{k} d\omega, \tag{2.53}$$

where ΔE_{co} and ΔE_{inc} denote net coherent and incoherent energies, respectively. Note that the second and the fourth terms in (2.52) are combined to yield -1 by (2.49). Leaving these terms separated is to distinguish the reflected coherent energy, i.e. the first two terms on the right-hand side in (2.52), from the transmitted one, i.e. the last two terms. Since net energy can be attributed to two factors such as the acoustic velocity jump due to unsteady heat release and the unsteady motion of flame wrinkling (as for unsteady motion effect, see also Crighton *et al.* 1992, chapter 14, which describes how a source in unsteady motion modifies the amplitude of sound field), coherent energy is further broken into the form

$$\Delta E_{co} = \Delta_J(E_{co}) + \Delta_w(E_{co}), \tag{2.54}$$

where the first term is due to the acoustic velocity jump

$$\begin{aligned}
\Delta_J(E_{co}) & = |\langle V(\mathbf{k}_0, \omega_0) \rangle|^2 - |\langle V(\mathbf{k}_0, \omega_0) \rangle|_{\beta=0}^2 \\
& \quad + \operatorname{Re}(q_0^{(2)}/|q_0^{(2)}|) (|\langle T(\mathbf{k}_0, \omega_0) \rangle|^2 - |\langle T(\mathbf{k}_0, \omega_0) \rangle|_{\beta=0}^2),
\end{aligned}$$

and the second term is due to the flame wrinkling, which accounts for both *temporal* (unsteady motion) and *spatial wrinkling* of flame fronts

$$\Delta_w(E_{co}) = \int_{\omega} \int_{\mathbf{k}} \int_{\mathbf{k}} \text{Re} [H_{\beta=0}(\mathbf{k}, \mathbf{k}_0, \omega, \omega_0)] W(\mathbf{k}_0 - \mathbf{k}, \omega_0 - \omega) d\mathbf{k} d\omega.$$

Net incoherent energy is also attributed to the velocity jump and the wrinkling effects.

$$\Delta E_{inc} = \Delta_J(E_{inc}) + \Delta_w(E_{inc}) \quad (2.55)$$

$$\begin{aligned} \Delta_J(E_{inc}) &= \int_{\omega} \int_{|\mathbf{k}| < |\omega|/c_1} \int_{|\mathbf{k}| < |\omega|/c_1} [\sigma_R(\mathbf{k}, \mathbf{k}_0, \omega, \omega_0) - \sigma_R(\mathbf{k}, \mathbf{k}_0, \omega, \omega_0)_{\beta=0}] d\mathbf{k} d\omega \\ &\quad + \int_{\omega} \int_{|\mathbf{k}| < |\omega|/c_2} \int_{|\mathbf{k}| < |\omega|/c_2} [\sigma_T(\mathbf{k}, \mathbf{k}_0, \omega, \omega_0) - \sigma_T(\mathbf{k}, \mathbf{k}_0, \omega, \omega_0)_{\beta=0}] d\mathbf{k} d\omega, \\ \Delta_w(E_{inc}) &= \int_{\omega} \int_{|\mathbf{k}| < |\omega|/c_1} \int_{|\mathbf{k}| < |\omega|/c_1} \sigma_R(\mathbf{k}, \mathbf{k}_0, \omega, \omega_0)_{\beta=0} d\mathbf{k} d\omega \\ &\quad + \int_{\omega} \int_{|\mathbf{k}| < |\omega|/c_2} \int_{|\mathbf{k}| < |\omega|/c_2} \sigma_T(\mathbf{k}, \mathbf{k}_0, \omega, \omega_0)_{\beta=0} d\mathbf{k} d\omega. \end{aligned}$$

3. Results and discussions

3.1. Non-dimensional parameters for the acoustic energy budget under the Gaussian statistics of flame height

The formulations for acoustic energy budget derived in the previous section are generalized ones in a sense that they are expressed in terms of the flame height correlation function W that allows any specific description of flame height statistics regardless of whether it follows a standard Gaussian statistics or not. (As for the correlation function, see (2.38) and its related context.) The flame height statistics in this section is assumed to follow the Gaussian characteristics to exemplify a quantitative demonstration of net acoustic energy budget. The flame height correlation function with the Gaussian distribution is of the form

$$\tilde{W}(\boldsymbol{\xi}, \eta) = \langle h(\mathbf{r}_1, t_1)h(\mathbf{r}_2, t_2) \rangle = \sigma^2 e^{-|\boldsymbol{\xi}|^2/l_c^2 - \eta^2/t_c^2} (\boldsymbol{\xi} = \mathbf{r}_1 - \mathbf{r}_2, \eta = t_1 - t_2), \quad (3.1)$$

where the correlation length l_c represents how far a signal, i.e. flame height, spreads its influence to its neighbouring points while the correlation time t_c represents how long a signal keeps its information in a subsequent time. In other words the correlation length controls a spatial variation of flame height along the surface and a larger l_c makes less spatial variation of flame height along the flame surface while the correlation time controls the rate of change of flame height with time and a larger t_c makes less temporal variation of flame height at a given location of flame surface.

Equation (3.1) leads the power spectrum of flame height to the form

$$W(\mathbf{k}, \omega) = \frac{1}{(2\pi)^3} \int_{\boldsymbol{\xi}} \int_{\eta} \tilde{W}(\boldsymbol{\xi}, \eta) e^{-i(\mathbf{k} \cdot \boldsymbol{\xi} - \omega\eta)} d\eta d\boldsymbol{\xi} = \frac{\sigma^2 t_c l_c^2}{8\pi^{3/2}} e^{-[(\omega t_c)^2 + (|\mathbf{k}| l_c)^2]/4} \quad (3.2)$$

which implies that a Gaussian correlation function yields a Gaussian power spectrum. Note that if a surface is stationary, the correlation time goes to infinity ($t_c \rightarrow \infty$). Hence

$$W(\mathbf{k}, \omega) = W(\mathbf{k})\delta(\omega) \quad \text{with} \quad W(\mathbf{k}) = \frac{(\sigma l_c)^2}{4\pi} e^{-(|\mathbf{k}| l_c)^2/4} \quad (3.3)$$

using $(t_c/\sqrt{\pi}) \exp[-(\omega t_c)^2] \rightarrow \delta(\omega)$ as $t_c \rightarrow \infty$ (Kevorkian 2000, p. 580). Calculation of net acoustic energy requires triple integrations over \mathbf{k} and ω , as seen in (2.47). With the flame height statistics following the Gaussian distribution as in (3.1), such triple integrations can be reduced to double integrations by utilizing a polar transform, $k_x = k \cos \theta$ and $k_y = k \sin \theta$. For instance, using a polar transform for the integration of FW in (2.47) yields:

$$\begin{aligned}
 & D(\mathbf{k}_0, \omega_0) \int_{\omega} \int_{\mathbf{k}} F(\mathbf{k}, \mathbf{k}_0, \omega, \omega_0, \omega_0) W(\mathbf{k}_0 - \mathbf{k}, \omega_0 - \omega) d\mathbf{k} d\omega \\
 &= \frac{2\tilde{q}_0^{(1)} \tilde{\sigma}^2}{\Lambda [\Lambda^{-1} \tilde{q}_0^{(1)} + \tilde{q}_0^{(2)} + \tilde{\beta}(\tilde{\omega}_0)]^2} \\
 & \times \left[\begin{aligned} & -\frac{4\tilde{\beta}(\tilde{\omega}_0)}{\tilde{l}_c^2} + \frac{\tilde{l}_c^2 e^{-(k_0 \tilde{l}_c)^2/4}}{4\pi^{1/2}} \times \int_{\omega=-\infty}^{\infty} \\ & \int_{k=0}^{\infty} \left(2\tilde{C}_{10}(k, \omega) I_0(k \tilde{k}_0 \tilde{l}_c^2/2) + 2k \tilde{k}_0 \tilde{C}_{11}(k, \omega) I_1(k \tilde{k}_0 \tilde{l}_c^2/2) \right) \\ & \left(+ (k \tilde{k}_0)^2 \tilde{C}_{12}(k, \omega) [I_0(k \tilde{k}_0 \tilde{l}_c^2/2) + I_2(k \tilde{k}_0 \tilde{l}_c^2/2)] \right) k e^{-[(k \tilde{l}_c)^2 + (\tilde{\omega}_0 - \omega)^2]/4} d\mathbf{k} d\omega \end{aligned} \right] \quad (3.4)
 \end{aligned}$$

where coefficients \tilde{C}_{10} , \tilde{C}_{11} , \tilde{C}_{12} are functions of k , ω , β , Λ

$$\begin{aligned}
 & \tilde{C}_{10}(k, \omega) \\
 &= \chi^{-1} \left(\begin{aligned} & \left[(1 - \Lambda^{-1}) \tilde{q}_0^{(2)} + \tilde{\beta}(\tilde{\omega}_0) \right] \left(\tilde{q}_k^{(1)} (\tilde{q}_0^{(2)} + \tilde{\beta}(\tilde{\omega}_0)) [(\Lambda - 1) \tilde{q}_k^{(2)} + \Lambda \tilde{\beta}(\omega)] \right) \\ & \left(+ \frac{\omega}{\tilde{\omega}_0} \chi + \frac{\tilde{\omega}_0}{\omega} \tilde{\beta}(\omega) \tilde{q}_k^{(1)} \tilde{q}_k^{(2)} \right) \\ & \left(+ \tilde{q}_0^{(2)} \tilde{\beta}(\tilde{\omega}_0) \left[\frac{\omega}{\tilde{\omega}_0} (\tilde{q}_k^{(1)} + \tilde{q}_k^{(2)}) (\tilde{q}_0^{(2)} + \tilde{\beta}(\tilde{\omega}_0)) - \tilde{q}_k^{(2)} \tilde{\beta}(\omega) \right] \right) \end{aligned} \right), \quad (3.5)
 \end{aligned}$$

$$\begin{aligned}
 & \tilde{C}_{11}(k, \omega) \\
 &= \chi^{-1} \left(\begin{aligned} & (1 - \Lambda^{-1}) [\tilde{q}_0^{(2)} \tilde{\beta}(\tilde{\omega}_0) + \tilde{q}_k^{(2)} \tilde{\beta}(\omega) - \frac{\omega}{\tilde{\omega}_0} (\tilde{q}_k^{(1)} + \tilde{q}_k^{(2)}) (\tilde{q}_0^{(2)} + \tilde{\beta}(\tilde{\omega}_0))] \\ & - \frac{\tilde{\omega}_0}{\omega} [(1 - \Lambda^{-1}) \tilde{q}_0^{(2)} + \tilde{\beta}(\tilde{\omega}_0)] (\tilde{q}_k^{(1)} + \tilde{q}_k^{(2)} + \tilde{\beta}(\omega)) \end{aligned} \right),
 \end{aligned}$$

$$\tilde{C}_{12}(k, \omega) = -(1 - \Lambda^{-1})^2 \chi^{-1}, \quad \chi(k, \omega) = \Lambda^{-1} \tilde{q}_k^{(1)} + \tilde{q}_k^{(2)} + \tilde{\beta}(\omega)$$

$$\tilde{q}_0^{(1)} = (1 - \tilde{k}_0^2)^{1/2}, \quad \tilde{q}_0^{(2)} = (\Lambda^{-1} - \tilde{k}_0^2)^{1/2}, \quad \tilde{q}_k^{(1)} = \left[\left(\frac{\omega}{\tilde{\omega}_0} \right)^2 - k^2 \right]^{1/2},$$

$$\tilde{q}_k^{(2)} = \left[\Lambda^{-1} \left(\frac{\omega}{\tilde{\omega}_0} \right)^2 - k^2 \right]^{1/2}$$

$$\tilde{\beta}(\omega) = \frac{\omega}{\tilde{\omega}_0} \left[\frac{\alpha}{2} (\gamma - 1) - \gamma - i(\gamma - 1)\theta \tau \omega \right] (1 - \Lambda^{-1}) M_S.$$

Equation (3.4) introduces five non-dimensional parameters: the r.m.s. flame height $\tilde{\sigma}$ ($= K_0 \sigma$), the correlation length of flame height \tilde{l}_c ($= K_0 l_c$), the frequency ratio \tilde{f}_0 ($= \tilde{\omega}_0 / (2\pi) = f_0 / f_c$) ($f_c = 1/t_c$: correlation frequency of flame surface), the time ratio of the flame's diffusion to correlation time τ ($= t_r / t_c$), the polar angle of incidence $\phi_0^{(1)}$ ($= \arcsin \tilde{k}_0$ with $\tilde{k}_0 = k_0 / K_0$).

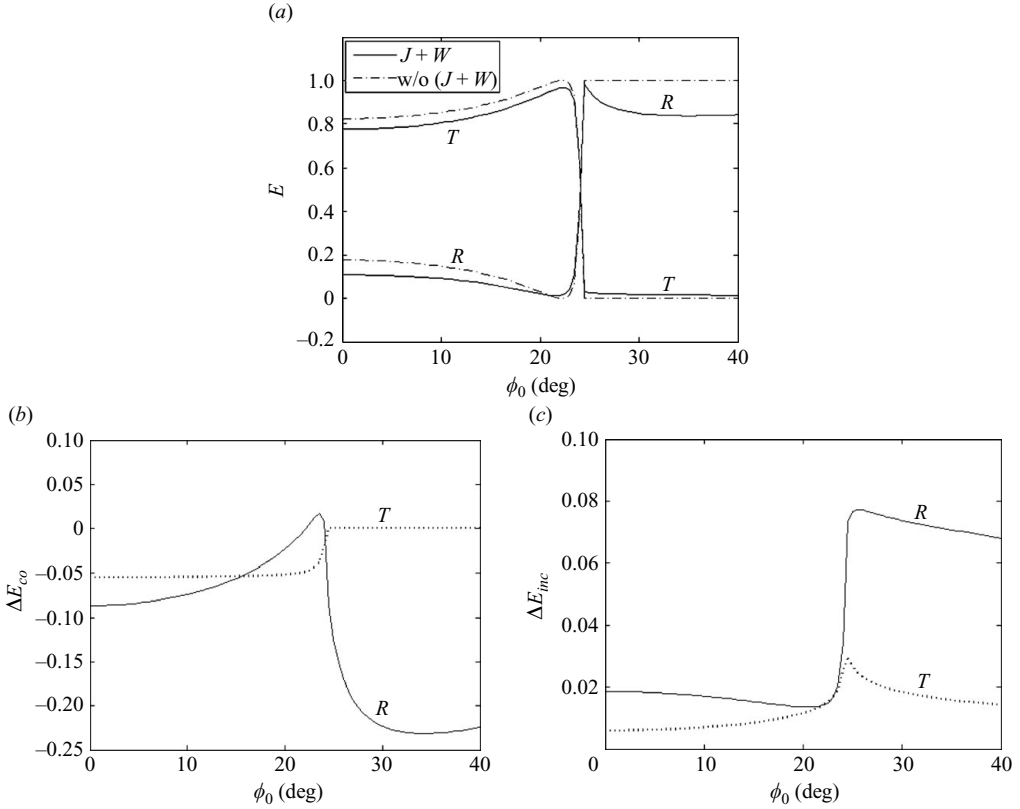


FIGURE 2. Dependence of the reflected and transmitted acoustic energy upon the incidence angle ($\tilde{\sigma} = 0.3$, $\tilde{l}_c = 2$, $\tilde{f}_0 = \tau = 0.1$; J : jump effect, W : wrinkling effect).

3.2. Numerical simulation of the scattered acoustic energy budget

The integrals in (2.54) and (2.55) were all converted to double integrals, as demonstrated in the previous section, and then numerically integrated using Mathematica to illustrate the characteristics of the scattered acoustic energy budget such as the reflected energy versus transmitted energy, coherent energy versus incoherent energy due to the jump effect versus wrinkling effect. The accuracy of numerical integrations was controlled and checked by the ‘digits of precision’. Setting the digits of precision to five or higher guaranteed that the numerically integrated values converge with a normalized variation of less than 10^{-4} . The integral range of $-\infty < \omega < \infty$ was approximated by $\tilde{\omega}_0 - \Delta\omega < \omega < \tilde{\omega}_0 + \Delta\omega$ as the integrals have the $\exp[-(\tilde{\omega}_0 - \omega)^2/4]$ dependence which decays exponentially with ω^2 . Using $\Delta\omega = 35$ or higher guaranteed that the integration stays within a normalized variation of 10^{-4} . Accordingly, the calculation that follows used $\Delta\omega = 35$. Similarly, the integral range over k is approximated by $0 \leq k \leq \Delta\omega/\tilde{l}_c$ since $k\tilde{l}_c$ corresponds to $\omega - \tilde{\omega}_0$ as seen in $\exp\{-[(k\tilde{l}_c)^2 + (\tilde{\omega}_0 - \omega)^2]/4\}$. The dimensionless parameters have the ranges of $\tilde{\sigma} \leq 0.3$, $\tilde{l}_c \geq 1.5$, $0^\circ \leq \phi_0 \leq 40^\circ$, based on the restrictions on the flame height and slope in (2.20). $\tilde{f}_0 (= f_0/f_c)$ and $\tau (= t_r/t_c)$ range from 0.1 to 10 to examine the relative importance between f_0 and f_c or between t_r and t_c , respectively. The variables for β (the jump factor) in (3.5) take on the values of $\alpha = 2$, $\gamma = 1.4$, $\theta = 10$, $\Lambda = 6$, $M_S = 0.001$.

Figure 2(a) shows the dependence of the reflected and transmitted energies upon the incidence angle with and without the unsteady effects of jump, denoted by ‘ J ’,

and wrinkling, denoted by ' W '. The case without the unsteady effects represents a typical wave reflection and transmission behaviour. The reflected energy displays about 18 % of the incidence energy at normal incidence ($\phi_0 = 0^\circ$), and decreases with increasing the incidence angle (deviating more from normal incidence) until it reaches the Brewster angle at about 22° where no reflection occurs. (The Brewster angle is given by $\phi_B = \arctan(\Lambda^{-1/2}) = 22.2^\circ$.) The reflected energy then increases dramatically beyond the Brewster angle until it reaches the critical angle at about 24° , beyond which all the energy is reflected. (The critical angle is given by $\phi_{cr} = \arcsin(\Lambda^{-1/2}) = 24.1^\circ$.) The unsteady effects of the jump and wrinkling, however, cause the energy amplification and/or damping that modifies the reflected and transmitted acoustic energy as shown in figure 2(a).

Net coherent and incoherent energies are shown in figures 2(b) and 2(c). Figure 2(b) shows that the coherently reflected energy is damped at *off-critical* angles, i.e. the angles which are more than about 1° distant from the critical angle. Coherent damping of the reflected energy at normal incidence is about 8 % of the incidence energy and is then gradually reduced with an increasing incidence angle until the coherent damping is switched to coherent amplification near the critical angle. This coherent damping at *subcritical* angles, i.e. below the critical angle, appears to be more or less proportional to the original reflection energy, i.e. the 'w/o ($J + W$)' curve shown in figure 2(a). In other words, a nearly constant portion of the reflection energy is damped due to the unsteady effects.

Coherent amplification of the reflected energy near the critical angle in figure 2(b) is thought to result from the influence by the behaviour at the Brewster angle which is near the critical angle. At the Brewster angle the reflection energy can never be further damped since all the energy is already transmitted (across a plane surface) at the Brewster angle by its definition. Thus net reflection energy scattered by a wrinkled surface can only be produced. Such net energy production holds for its neighbouring angles including the critical angle in this study. Note that no coherent energy is transmitted beyond the critical angle as is the case of the transmission through a plane surface.

Figure 2(c) shows that incoherent energy is always produced for both reflected and transmitted fields. Note that some incoherent energy is still transmitted even at *supercritical* angles, i.e. beyond the critical angle, as opposed to zero transmission of coherent energy at supercritical angles as shown in figure 2(b). This is due to the fact that surface wrinkling, which produces incoherent energy, sometimes makes a local incidence angle subcritical even when the incidence angle from the mean surface is supercritical. These locally made subcritical angles allow some waves to be transmitted. Note also in figures 2(b) and 2(c) that coherent damping and incoherent production at supercritical angles are more pronounced than those at subcritical angles. This implies that a more oblique incident wave (with a supercritical incidence angle), which is disturbed transversely by the up-and-down motion (in an average sense) of a wrinkled flame, is more effectively scattered to damp coherent energy into incoherent energy than a less oblique incident wave (with a subcritical incidence angle) which is disturbed rather longitudinally.

The detailed energy budget is summarized in figure 3, which illustrates dominant processes that amplify and/or damp acoustic energy by the interaction with a turbulent flame. Net acoustic energy is caused by two effects: one is the acoustic velocity jump effect due to the flame's unsteady heat release, and the other is the wrinkling effect due to the flame's unsteady motion. Note that the wrinkling effect consists of two factors: temporal wrinkling and spatial wrinkling. Temporal

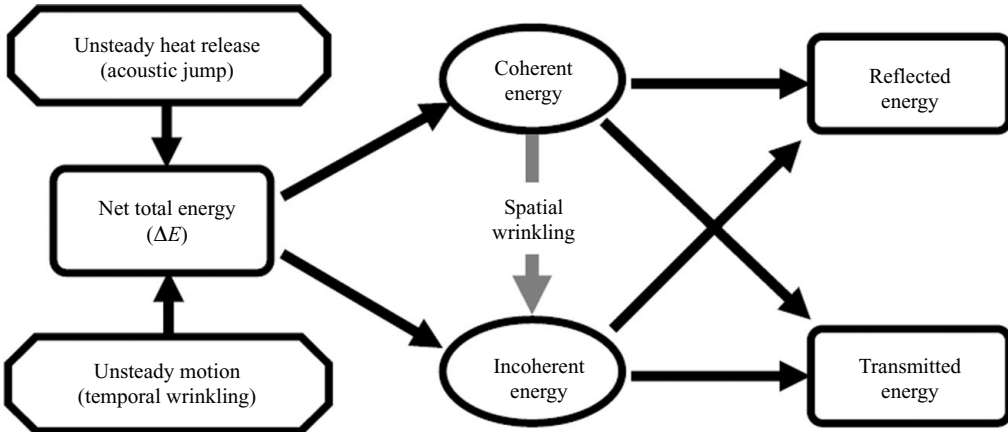


FIGURE 3. Dominant processes for amplification and/or damping of acoustic energy by the interaction with a turbulent flame.

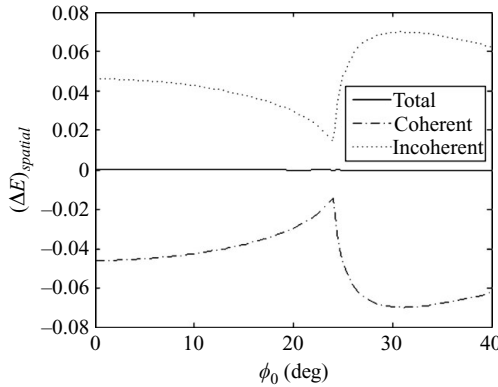


FIGURE 4. Acoustic energy balance for a stationary wrinkling surface ($\bar{\sigma} = 0.3, \tilde{l}_c = 2, \tilde{\beta} = 0$).

wrinkling is associated with unsteady motion of flame surface while spatial wrinkling is associated with spatial variation of a wrinkled surface that causes energy transfer from coherent to incoherent energy. Thus, spatial wrinkling redistributes acoustic energy between coherent and incoherent fields and does not alter total energy, as shown in figure 4 where $(\Delta E)_{spatial}$ denotes net energy change of a spatially wrinkled but stationary surface with no heat release.

Note also in figure 4 (and subsequent figures) that the peaks, i.e. discontinuities in slope, at the critical angle are caused by the *cut-off* phenomena where no wave is transmitted. It is mathematically explained by the fact that a vertical wavenumber $\tilde{q}_0^{(2)}$ in (3.5) is a real value for a subcritical angle but becomes an imaginary value for a supercritical angle. In other words, the argument of $\tilde{q}_0^{(2)}$ makes a jump from 0° to 90° in a complex domain when crossing the critical angle (this discontinuous behaviour was also observed in the high-frequency acoustic wave analysis by Lieuwen & Cho 2005).

Figure 5 shows net total energy due to the jump and wrinkling effects and respective contributions from coherent and incoherent fields. Figure 5(a) shows that coherent energy is damped and incoherent energy is amplified for the entire range of the incidence angle. It also shows that total energy is significantly damped for a small

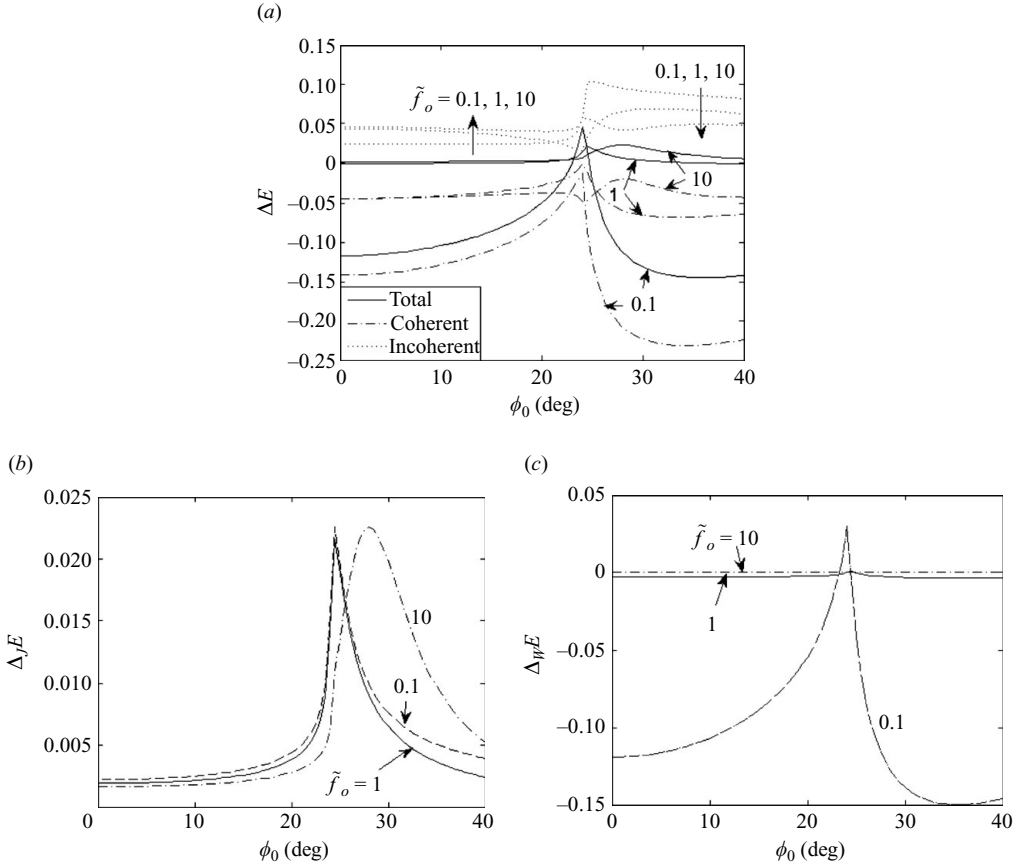


FIGURE 5. Jump and wrinkling effects upon net energy as a function of the incidence angle for various \tilde{f}_0 ($\tau = 1$, $\tilde{\sigma} = 0.3$, $\tilde{l}_c = 2$).

frequency ratio ($\tilde{f}_0 = 0.1$) at off-critical angles. Such damping is caused by the wrinkling effect as shown in figure 5(c). (Note that the wrinkling effect here is temporal wrinkling, not spatial wrinkling as explained previously.) Total energy amplification near the critical angle for $\tilde{f}_0 = 0.1$ is, however, attributable almost equally to the jump and the wrinkling effects, as shown in figures 5(b) and 5(c).

Figure 5(a) also shows that, for a larger frequency ratio ($= 1, 10$), net total energy becomes much smaller and less sensitive to the incidence angle. This is because the wrinkling effect is greatly suppressed compared to the case of $\tilde{f}_0 = 0.1$ as shown in figure 5(c). Such dominance of the wrinkling effect to the jump effect for a small frequency ratio arises from the fact that a smaller frequency ratio ($= f_0/f_c$) yields a larger characteristic frequency of a flame surface f_c leading to an enhanced wrinkling effect. With large frequency ratios ($= 1, 10$), however, the jump effect is comparable or dominant to the wrinkling effect as the wrinkling effect is greatly reduced while the jump effect varies little as shown in figure 5(b). These figures also show that the jump effect acts as a source of acoustic energy amplification for the entire range of the incidence angle while the wrinkling effect acts as a source of damping for almost entire range of the incidence angle except for the near-critical angle where amplification occurs.

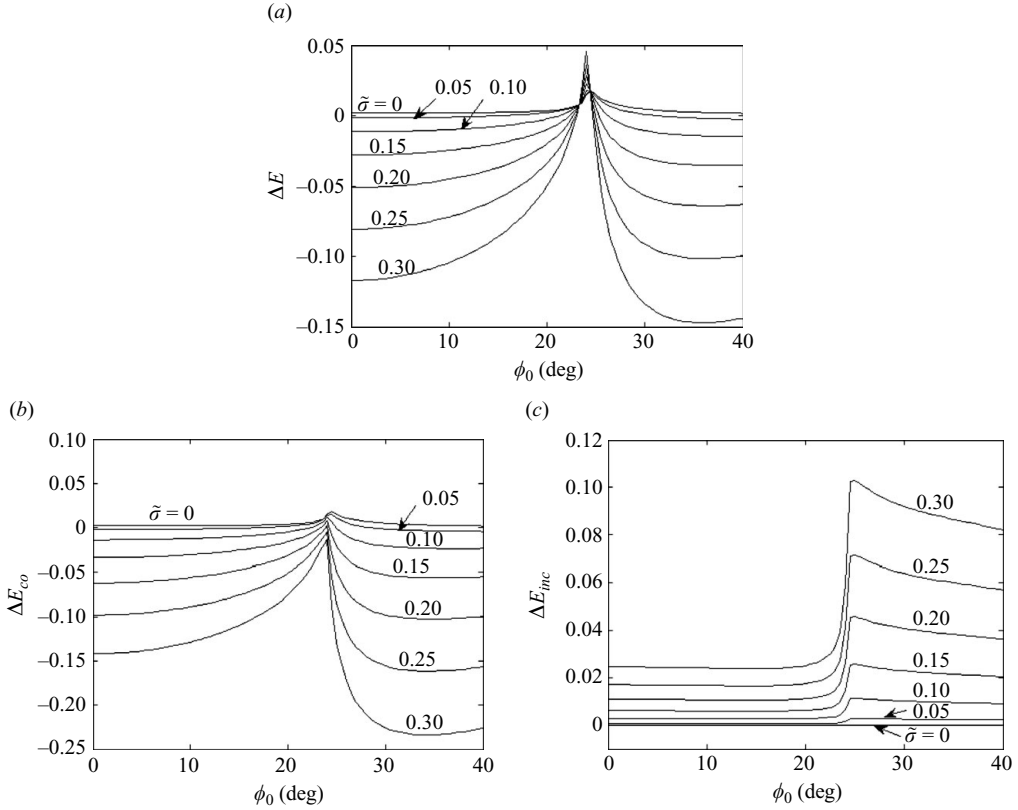


FIGURE 6. Dependence of net acoustic energy upon the flame's r.m.s. height as a function of the incidence angle ($\tilde{f}_0 = \tau = 0.1$, $\tilde{l}_c = 2$).

Figure 6 shows how net acoustic energy varies with the flame's r.m.s. height. It is observed that net total, coherent and incoherent energies vary with the square of the r.m.s. height. (Note that coherent and incoherent energies in (2.47) have a linear dependence on the power spectrum W , which is proportional to the square of the r.m.s. height as in (3.2).) Figure 6(a) shows that, when some wrinkling exists ($\tilde{\sigma} > 0$), net total energy is amplified near the critical angle and damped at off-critical angles. For a flat surface with no roughness ($\tilde{\sigma} = 0$), net total energy is still produced by the jump effect due to unsteady heat release. Such net energy is purely coherent as a flat surface produces no incoherent energy, as shown in figure 6(c). This coherent amplification near the critical angle for a flat surface was also demonstrated by Lieuwen & Cho (2005, figure 10). With increasing r.m.s. height, the coherent damping and incoherent production, as shown in figures 6(b) and 6(c), are augmented as the energy transfer from coherent field to incoherent field is more facilitated due to enhanced surface roughness. Incoherent production is more significant at supercritical angles than at subcritical angles in figure 6(c) as explained in figure 2.

Figure 7 shows the dependence of net energy upon the frequency and time ratios for a subcritical incidence angle, 10° . Maximum damping of 10% occurs at $\tilde{f}_0 = 0.1$, as shown in figure 7(a), which results from 12% of coherent damping and 2% of incoherent production, as shown in figures 7(b) and 7(c). Such damping at a small frequency ratio (< 1) is mainly due to the wrinkling effect with a negligible jump

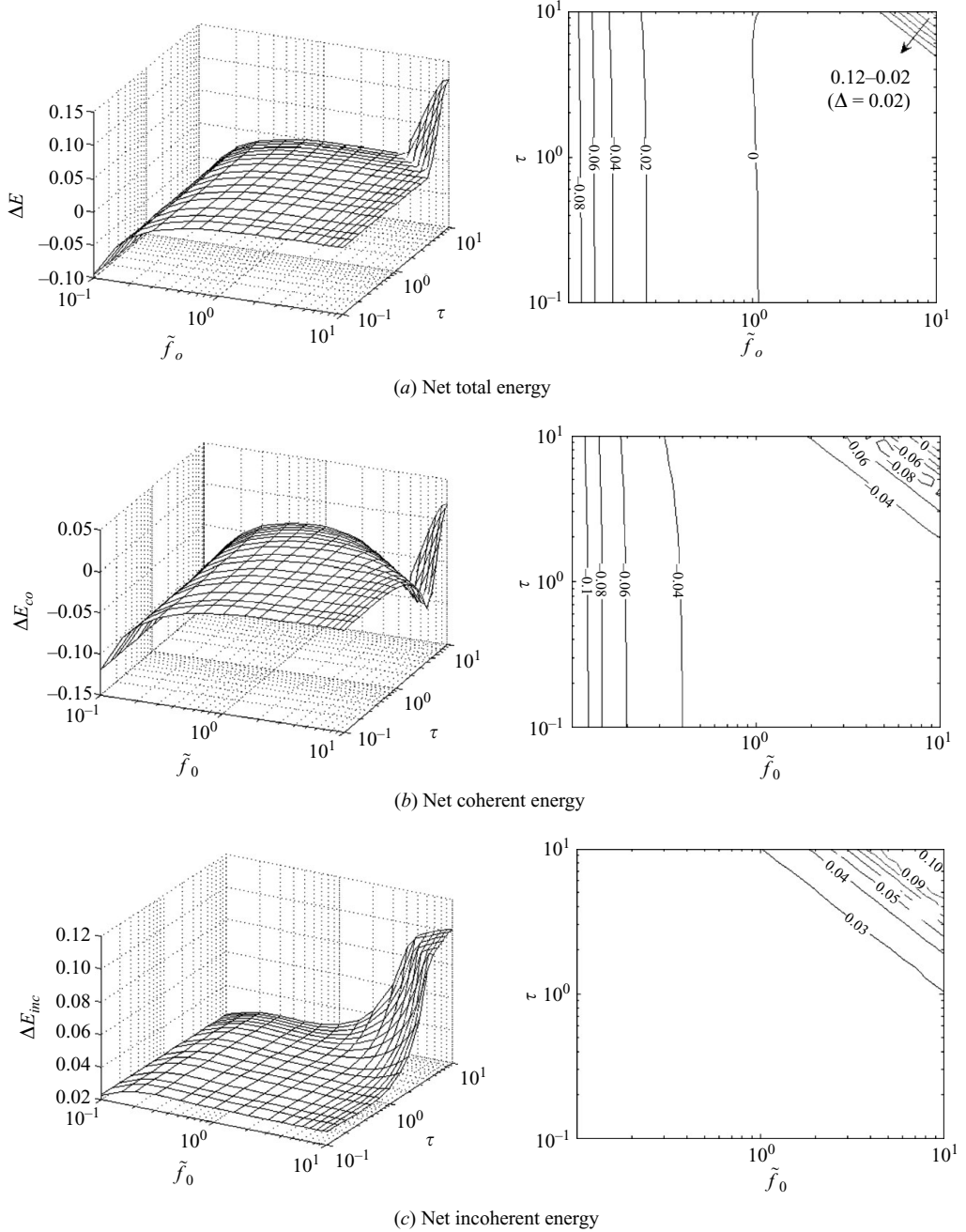


FIGURE 7. For caption see facing page.

effect, as shown in figures 7(d) and 7(e). This follows from the same reasoning as made for figure 5; i.e. a smaller frequency ratio not only yields a relatively higher oscillation of a flame surface ($f_c > f_0$) which enhances unsteady wrinkling effect, but it also yields a smaller value of a jump factor β , because of $\tilde{\beta}(\tilde{\omega}_0) \sim f_0$ from (3.5), leading to a smaller jump effect. The jump effect, however, becomes more pronounced on both coherent and incoherent energies for larger frequency ratios

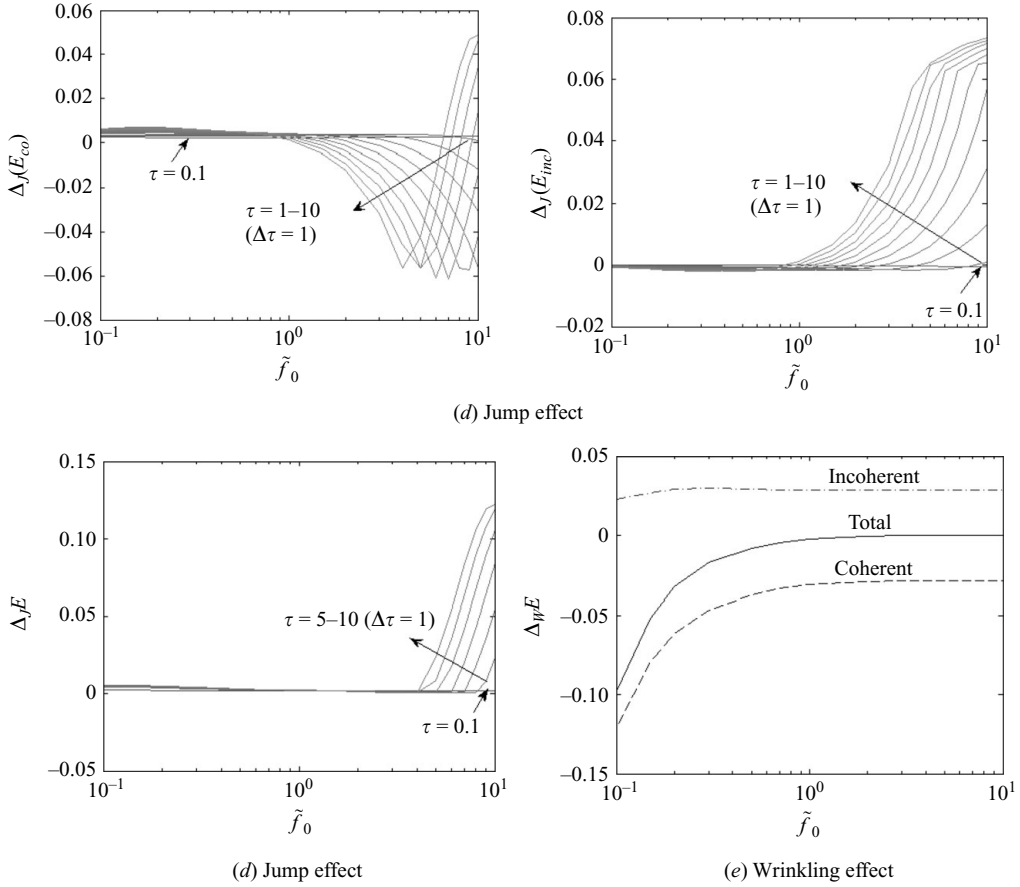


FIGURE 7. Dependence of net energy upon \tilde{f}_0 and τ at a subcritical angle ($\tilde{\sigma} = 0.3$, $\tilde{l}_c = 1.5$, $\phi_0 = 10^\circ$).

(> 1), as shown in figure 7(d), especially for a large time ratio τ because more heat is released with an increase in the diffusion time of flame.

For a frequency ratio of $O(1)$, net total energy is negligibly small in figure 7(a) because coherent damping is almost as large as incoherent production as shown in figures 7(b) and 7(c). Coherent energy is damped in most regions except for the largest frequency and time ratios ($\tilde{f}_0 \approx 10$, $\tau \approx 10$) in figure 7(b), and incoherent energy is also produced most for the largest frequency and time ratios as shown in figure 7(c). Such incoherent energy production exhibits a noticeable increase and subsequent saturation with frequency and time ratios greater than $O(1)$. In figures 7(d) and 7(e) the jump effect dominates the wrinkling effect when the frequency ratio $\gg 1$, acting as a source of amplification in net total energy, while the wrinkling effect dominates the jump effect when the frequency ratio is less than 1, acting as a source of damping.

It is noteworthy to compare the calculated incoherent energy in figure 7(c) with the experimental data reported by Lieuwen *et al.* (2002) as shown in figure 8. They performed measurements of acoustic wave scattering from a rim-stabilized turbulent premixed flame. Figure 8(a) shows the power spectral density (PSD) of the sidebands of the scattered acoustic fields where the sidebands become wider with driving

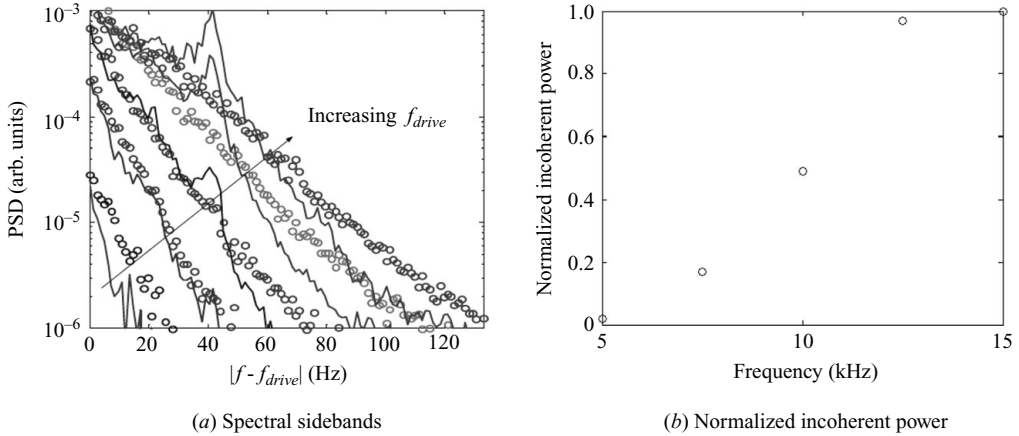


FIGURE 8. Dependence of incoherent power in spectral sidebands upon driving frequency ($\phi = 0.93$) (courtesy of Lieuwen *et al.* 2002).

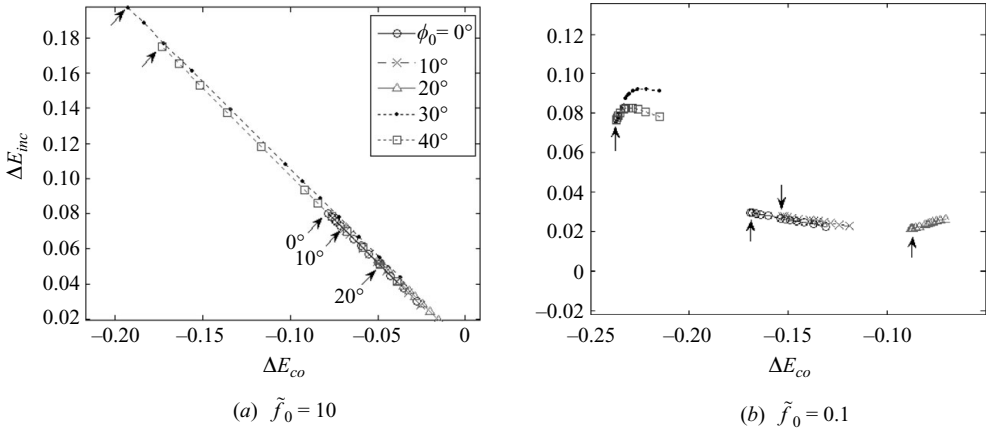


FIGURE 9. Correlation between net coherent and incoherent energies for various \tilde{f}_0 ($\tilde{\sigma} = 0.3$, $\tau = 0.1$). Each curve for a given ϕ_0 is drawn for various \tilde{l}_c from 1.5 to 8 with arrows indicating the points of $\tilde{l}_c = 8$.

(incident) frequency f_{drive} . The generation of sidebands with a broadband spectrum is attributable to the Doppler frequency shift due to random oscillation of turbulent flame surfaces. Figure 8(b) shows the dependence of incoherent scattered power upon an incident frequency. The incoherent scattered power was obtained by evaluating the area under the PSD in the relevant spectral region from figure 8(a) with normalization by the power at $f_{drive} = 15$ kHz. The incoherent scattered power is increased and saturated with driving frequency, which shows a qualitative agreement with the pattern delineated by the calculated incoherent energy in figure 7(c) even though this experimental data was measured at a rather higher frequency range which is beyond the applicable regime of the present analysis.

Figure 9 illustrates correlation between net coherent and incoherent energies. The case of $\tilde{f}_0 = 10$ in figure 9(a) displays a linear correlation with a slope of -1 , which implies that, for a large frequency ratio, total energy varies little with the incidence angle and the correlation length. On the other hand, the case of $\tilde{f}_0 = 0.1$ in figure

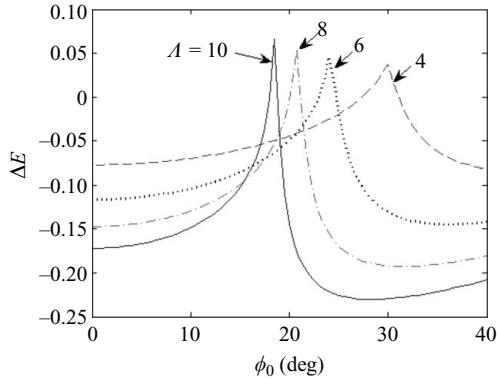


FIGURE 10. Dependence of net acoustic energy upon temperature ratio ($\tilde{\sigma} = 0.3$, $\tilde{f}_0 = 0.1$, $\tilde{l}_c = 2$, $\tau = 1$).

9(b) displays a poor correlation, which implies that net total energy varies much with the incidence angle and the correlation length for a small frequency ratio (see figure 5(a) where net total energy varies little with the incidence angle at $\tilde{f}_0 = 10$ while it varies significantly at $\tilde{f}_0 = 0.1$). Figure 10 shows the effect of temperature ratio upon net total energy. The peak in net total energy occurs at a lower incidence angle with a larger temperature ratio because the critical angle decreases with an increasing temperature ratio. Also note that a larger temperature ratio enhances energy amplification as well as damping, i.e. amplification at the critical angle and damping at off-critical angles are both enhanced with an increasing temperature ratio.

4. Concluding remarks

Acoustic wave-turbulent flame interactions in the long-wavelength regime were analysed using SPM up to the second order to derive the generalized formulations of net coherent and incoherent acoustic energies for the reflected and transmitted scattered fields. Net acoustic energy is caused by two effects: (i) the acoustic velocity jump due to the flame's unsteady burning rate and (ii) the flame's wrinkling due to its unsteady motion. (Thus, acoustic energy is conserved in the case of no unsteady effects considered.) Five dimensionless parameters that govern net acoustic energy were derived based on the Gaussian statistics for flame height: the r.m.s. height and the correlation length of flame front, the frequency ratio of the incidence frequency to the flame's correlation frequency, the time ratio of the flame's diffusion to correlation time and the incidence angle. Acoustic energy amplification occurs for a large frequency ratio and time ratio ($\gg 1$) while damping occurs for a small frequency ratio ($\ll 1$) at off-critical incidence angles. Total acoustic energy is always amplified near the critical angle. However, little change in total acoustic energy was observed for a frequency ratio of $O(1)$. The relative contribution of the jump effect (due to unsteady heat release) and the wrinkling effect (due to unsteady motion) to net total energy is controlled mainly by the frequency ratio: the jump effect dominates the wrinkling effect when the frequency ratio $\gg 1$, acting as a source of amplification in net total energy, while the wrinkling effect dominates the jump effect when the frequency ratio $\ll 1$, acting as a source of damping except for the near-critical incidence angle where the wrinkling effect also amplifies acoustic energy. Acoustic energy amplification and/or damping is augmented with increasing r.m.s. height and temperature ratio.

The energy transfer from coherent to incoherent energy is due to the flame surface wrinkling and is enhanced with the square of the flame's r.m.s. height. Future works will incorporate into the present analysis the vortex – turbulent flame interactions to examine the effect of vortical fluctuations excited at the flame on the coherent and incoherent acoustic energies amplification and/or damping.

The author would like to give a grateful acknowledgement to Professor Tim C. Liewen at Georgia Institute of Technology for his fruitful comments and discussions with constant encouragement.

Appendix A. Formulation of averaged quantities

A time-averaged intensity of multi-frequency waves, i.e. $p(t) = Re[\int_{\omega} P(\omega)e^{-i\omega t} d\omega]$ and $v(t) = Re[\int_{\omega} V(\omega)e^{-i\omega t} d\omega]$, can be evaluated by

$$\begin{aligned}
 I_{av,time} &= \lim_{T \rightarrow \infty} \frac{1}{T} \int_{-T/2}^{T/2} p(t)v(t) dt \\
 &= \frac{1}{4} \int_{\omega} \int_{\omega'} P(\omega) \left[V(\omega') \left(\lim_{T \rightarrow \infty} \frac{1}{T} \int_{-T/2}^{T/2} e^{-i(\omega+\omega')t} dt \right) + V^*(\omega') \right. \\
 &\quad \left. \times \left(\lim_{T \rightarrow \infty} \frac{1}{T} \int_{-T/2}^{T/2} e^{-i(\omega-\omega')t} dt \right) \right] d\omega' d\omega + \text{Complex Conjugate} \\
 &= \frac{1}{4} \int_{\omega} P(\omega) \left(\int_{\omega' \rightarrow -\omega} V(\omega') d\omega' + \int_{\omega' \rightarrow \omega} V^*(\omega') d\omega' \right) d\omega + \text{Complex Conjugate} \\
 &= \frac{1}{2} Re \left\{ \int_{\omega} P(\omega) \left(\int_{\omega' \rightarrow \omega} [-V(-\omega') + V^*(\omega')] d\omega' \right) d\omega \right\} \quad (A 1)
 \end{aligned}$$

where the following equation is used:

$$\lim_{T \rightarrow \infty} \frac{1}{T} \int_{-T/2}^{T/2} e^{-2i\omega t} dt = \begin{cases} \lim_{T \rightarrow \infty} \frac{\sin(\omega T)}{\omega T} = 1 & (\omega = 0) \\ 0 & (\omega \neq 0) \end{cases} \quad (A 2)$$

For waves of discrete frequencies, i.e. $P(\omega) = \sum_m P_m \delta(\omega - \omega_m)$ and $V(\omega) = \sum_n V_n \delta(\omega - \omega_n)$, (A 1) leads to

$$\begin{aligned}
 I_{av,time} &= \frac{1}{2} \sum_m \sum_n Re \left\{ \int_{\omega} P_m \delta(\omega - \omega_m) (-V_n \delta_{\omega(-\omega_n)} + V_n^* \delta_{\omega\omega_n}) d\omega \right\} \\
 &= \frac{1}{2} \sum_m \sum_n Re \left\{ P_m (-V_n \delta_{\omega_m(-\omega_n)} + V_n^* \delta_{\omega_m\omega_n}) \right\} = \frac{1}{2} \sum_n Re(P_n V_n^*) \quad (A 3)
 \end{aligned}$$

which is a well-known formulation. Note that Kronecker's delta function, $\delta_{\omega\omega_n}$, results from the fact that $\int_{\omega' \rightarrow \omega} \delta(\omega' - \omega_n) d\omega' = 1$ for $\omega = \omega_n$, or 0 for $\omega \neq \omega_n$.

Similarly, for multi-frequency and multi-directional waves expressed as

$$\begin{aligned}
 \tilde{p}(\mathbf{R}, t) &= Re \left[\int_{\omega} \int_{\mathbf{k}} \int P(\mathbf{k}, \omega, z) e^{i(\mathbf{k} \cdot \mathbf{r} - \omega t)} d\mathbf{k} d\omega \right], \quad (A 4) \\
 \tilde{v}(\mathbf{R}, t) &= Re \left[\int_{\omega} \int_{\mathbf{k}} \int V(\mathbf{k}, \omega, z) e^{i(\mathbf{k} \cdot \mathbf{r} - \omega t)} d\mathbf{k} d\omega \right]
 \end{aligned}$$

with $\tilde{p} = p/|P_T|$ and $\tilde{\mathbf{v}} = \mathbf{v}/c_1$, a time and surface-averaged intensity is of the form

$$\begin{aligned} \mathbf{I}_{av} &= \lim_{A,T \rightarrow \infty} \frac{1}{AT} \int_{|x|,|y| \leq \sqrt{A}/2} \int_{-T/2}^{T/2} \tilde{p}(\mathbf{R}, t) \tilde{\mathbf{v}}(\mathbf{R}, t) dt d\mathbf{r} \\ &= \frac{1}{2} Re \left\{ \int_{\omega} \int_{\mathbf{k}} \int P(\mathbf{k}, \omega, z) \left[\int_{\omega' \rightarrow \omega} \int_{\mathbf{k}' \rightarrow \mathbf{k}} \int (-\mathbf{V}(-\mathbf{k}', -\omega', z) \right. \right. \\ &\quad \left. \left. + \mathbf{V}^*(\mathbf{k}', \omega', z)) d\mathbf{k}' d\omega' \right] d\mathbf{k} d\omega \right\} \end{aligned} \quad (\text{A } 5)$$

where the surface average is taken over a mean flame surface. Note that (A 5) is valid for both deterministic and random variables of P and \mathbf{V} . For a random field, e.g. scattered by a randomly moving surface which makes the scattered pressure and velocity also random, its stochastic characteristics can be described by utilizing the ensemble average.

$$\langle \mathbf{I}_{av} \rangle = \frac{1}{2} Re \left\{ \int_{\omega} \int_{\mathbf{k}} \int \left[\int_{\omega' \rightarrow \omega} \int_{\mathbf{k}' \rightarrow \mathbf{k}} \int \left(-\langle P(\mathbf{k}, \omega, z) \mathbf{V}(-\mathbf{k}', -\omega', z) \rangle \right) d\mathbf{k}' d\omega' \right] d\mathbf{k} d\omega \right\}. \quad (\text{A } 6)$$

REFERENCES

- BLOXSIDGE, G. J., DOWLING, A. P., HOOPER, N. & LANGHORNE, P. J. 1998 Active control of reheat buzz. *AIAA J.* **26** (7), 783–790.
- CHO, J. H. 2006 Analysis of the wave scattering from turbulent premixed flame. PhD Thesis, Georgia Institute of Technology.
- CHU, B. T. 1952 On the generation of pressure waves at a plane flame front. *Proc. Combust. Inst.* **4**, 603–612.
- CHU, B. T. & KOVASZNY, L. S. G. 1958 Nonlinear interactions in a viscous heat-conducting compressible gas. *J. Fluid Mech.* **3**, 494–514.
- CLAVIN, P., PELCE, P. & HE, L. 1990 One-dimensional vibratory instability of planar flames propagating in tubes. *J. Fluid Mech.* **216**, 299–322.
- CRIGHTON, D. G., DOWLING, A. P., FLOWCS WILLIAMS, J. E., HECKL, M. & LEPPINGTON, F. G. 1992 *Modern Methods in Analytical Acoustics*. Springer-Verlag.
- FLEIFIL, M., ANNASWAMY, A. M., GHONIEM, Z. A. & GHONIEM, A. F. 1996 Response of a laminar premixed flame to flow oscillations: a kinematic model and thermoacoustic instability results. *Combust. Flame* **106**, 487–510.
- KEVORKIAN, J. 2000 *Partial Differential Equations: Analytical Solution Techniques*. Springer-Verlag.
- LEDDER, G. & KAPILA, A. K. 1991 The response of premixed flames to pressure perturbations. *Combust. Sci. Tech.* **76**, 21–44.
- LIEUWEN, T. 2001a Theoretical investigation of unsteady flow interactions with a premixed planar flame. *J. Fluid Mech.* **435**, 289–303.
- LIEUWEN, T. 2001b Theory of high frequency acoustic wave scattering by turbulent flames. *Combust. Flame* **126** (1-2), 1489–1505.
- LIEUWEN, T. 2002 Analysis of acoustic wave interactions with turbulent premixed flames. *Proc. Combust. Inst.* **29**, 1817–1824.
- LIEUWEN, T. & CHO, J. H. 2005 Coherent acoustic wave amplification/damping by wrinkled flames. *J. Sound Vib.* **279**, 669–686.
- LIEUWEN, T., RAJARAM, R., NEUMEIER, Y. & NAIR, S. 2002 Measurements of incoherent acoustic wave scattering from turbulent premixed flames. *Proc. Combust. Inst.* **29**, 1809–1815.
- LIEUWEN, T. & YANG, V. 2005 *Combustion Instabilities in Gas Turbine Engines*. AIAA, Inc..
- MARKSTEIN, G. H. 1964 *Nonsteady Flame Propagation*. Pergamon Press.
- MCINTOSH, A. C. 1987 Combustion-acoustic interaction of a flat flame burner system enclosed within an open tube. *Combust. Sci. Tech.* **54**, 217–236.
- MCINTOSH, A. C. 1991 Pressure disturbances of different length scales interacting with conventional flames. *Combust. Sci. Tech.* **75**, 287–309.

- MCINTOSH, A. C. 1999 Deflagration fronts and compressibility. *Phil. Trans. R. Soc. London* **357**, 3523–3538.
- MCINTOSH, A. C. & WILCE, S. A. 1991 High frequency pressure wave interaction with premixed flames. *Combust. Sci. Tech.* **79**, 141–155.
- MCMANUS, K. R., POINSOT, T. J. & CANDEL, S. M. 1993 A review of active control of combustion instabilities. *Prog. Energy Combust. Sci.* **19**, 1–29.
- MEIROVITCH, L. 1971 *Analytical Methods in Vibrations*. Macmillan Company.
- OGILVY, J. A. 1991 *Theory of Wave Scattering from Random Rough Surfaces*. IOP Publishing.
- PETERS, N. & LUDFORD, G. S. S. 1983 The effect of pressure variations on premixed flames. *Combust. Sci. Tech.* **34**, 331–344.
- POINSOT, T. J. & CANDEL, S. M. 1988 A nonlinear model for ducted flame combustion instabilities. *Combust. Sci. Tech.* **61**, 121–153.
- POINSOT, T. J., TROUVE, A. C., VEYNANTE, D. P., CANDEL, S. M. & ESPOSITO, E. J. 1987 Vortex-driven acoustically coupled combustion instabilities. *J. Fluid Mech.* **177**, 265–292.
- PUTNAM, A. A. 1971 *Combustion Driven Oscillations in Industry*. American Elsevier.
- SEARBY, G. & CLAVIN, P. 1986 Weakly turbulent, wrinkled flames in premixed gases. *Combust. Sci. Tech.* **46**, 167–193.
- SEARBY, G. & ROCHWERGER, D. 1991 A parametric acoustic instability in premixed flames. *J. Fluid Mech.* **231**, 529–543.
- VORONOVICH, A. G. 1999 *Wave Scattering from Rough Surfaces*. Springer-Verlag.